Author/s:
Reser, DH;Majka, P;Snell, S;Chan, JMH;Watkins, K;Worthy, K;Quiroga, MDM;Rosa, MGP

Title:
Topography of claustrum and insula projections to medial prefrontal and anterior cingulate cortices of the common marmoset (Callithrix jacchus)

Date:
2017-04-15

Citation:
Reser, D. H., Majka, P., Snell, S., Chan, J. M. H., Watkins, K., Worthy, K., Quiroga, M. D. M. & Rosa, M. G. P. (2017). Topography of claustrum and insula projections to medial prefrontal and anterior cingulate cortices of the common marmoset (Callithrix jacchus). Journal of Comparative Neurology, 525 (6), pp.1421-1441. https://doi.org/10.1002/cne.24009.

Persistent Link:
https://hdl.handle.net/11343/291334

Topography of claustrum and insula projections to medial prefrontal and anterior cingulate cortex of the common marmoset (*Callithrix jacchus*)

David H. Reser[1,2], Piotr Majka[1,2,4], Shakira Snell[1], Jonathan Chan[1], Kirsty Watkins[1], Katrina Worthy[1], Maria Del Mar Quiroga[1], Marcello G.P. Rosa[1,2,3]

[1]Department of Physiology, Monash University, Clayton, VIC 3800 Australia

[2]Neuroscience Program, Biomedicine Research Institute, Monash University, Clayton, VIC 3800 Australia

[3]ARC Centre of Excellence for Integrative Brain Function, Monash University Node, Clayton, VIC 3800, Australia

[4]Nencki Institute of Experimental Biology, Polish Academy of Sciences, 3 Pasteur Street, 02-093 Warsaw, Poland

7175 Words

11 Figures

1 Table

Keywords: Cingulate Cortex; Medial Prefrontal Cortex; Claustrum; Resting State Networks; Marmoset; Neuroanatomy; Connections; RRID: SCR_014318; RRID:SCR_011010; RRID: SCR_014319; RRID: SCR_014198; RRID: SCR_014199; RRID: SCR_014317

List of abbreviations

A-P: Anterior to Posterior stereotaxic axis
BDA: Biotinylated dextran amine
BOLD: Blood oxygen level dependent
BVR: Basal vein of Rosenthal
CTB-a488: Cholera toxin B subunit conjugated to alexa488 fluorophore
CTB-g: Cholera toxin B subunit conjugated to gold nanoparticles
DAB: Diamino benzidine
DPX: Dibutyl phthalate + xylene
DY: Diamidino yellow
fMRI: Functional magnetic resonance imaging
Gu: Gustatory cortex
MD: Mediodorsal nucleus of the thalamus
MPFC: Medial prefrontal cortex
OPAI: Orbital periallocortical area
OPro: Orbital proisocortical area
PBS: Phosphate buffered saline
PFA: paraformaldehyde
ProM: Proisocortical motor region
VA: Ventral anterior nucleus of the thalamus
VAM: Vental anterior nucleus of the thalamus (medial subdivision)

Abstract:

The claustrum has been the subject of intense research interest in recent years, driven in large part by its extensive connections with various regions of the cerebral cortex, and by hypotheses surrounding its possible role in multimodal sensory and/or sensory-emotional integration. Here we employed neuroanatomical tracers to map projections from the claustrum-insular region to the medial prefrontal and anterior cingulate cortex of the common marmoset (*C. Jacchus*). These areas were selected based on their identification as 'hub' areas of the default mode and cortical salience networks, respectively. Microinjections of fluorescent tracers, along with gold nanoparticle conjugated cholera toxin B-subunit and biotinylated dextran amine, were placed in subdivisions of the anterior cingulate area 24, and in medial prefrontal areas 32 and 32V. The resulting distribution of transported label showed rostral-caudal and dorsal-ventral topographic arrangement of claustrum connections, and clear rostral-caudal topography of insular projections. Medial prefrontal connections were mainly restricted to a ventromedial strip located in the rostral half of the claustrum, with a second, smaller patch of cells in the caudal, ventrolateral portion. In contrast, injections into area 24 yielded dense, widespread connections from the dorsal claustrum, extending along its entire rostral-caudal length. Projections from the "classical" agranular, disgranular, and granular insular areas were sparse or non-existent in the areas 32 and 32V, with progressively increasing connections observed in more caudal tracer injections (i.e., in subdivisions of area 24). Transported label was observed in rostral peri-insular areas OPAI, OPro, and the insular proisocortex following all prefrontal injections. These data provide a structural connectivity foundation for interpretation of functional imaging studies, which often report activity in the "anterior insula" that may arise, in part, from claustrum and/or peri-insular projections to the anterior cingulate and medial prefrontal cortices.

Introduction:

In recent years, hypotheses surrounding the function of the mammalian claustrum have converged on two main ideas: that this structure has a primary role in polymodal sensory integration and binding (Smythies et al., 2012, 2014), or that it is primarily involved in selective attention and/or salience (Remedios et al., 2014; Reser et al., 2014; Goll et al., 2015; Patru and Reser, 2015a). Both of these general ideas are underpinned by the widespread connectivity of the claustrum with the cerebral cortex. Indeed, the claustrum has been identified as one of the most highly connected regions of the human (Torgerson and Van Horn, 2014) and rodent (Bota et al., 2015) brain. Another attention-relevant hypothesis regarding claustrum function revolves around coordination of sensory and motor areas between the cerebral hemispheres to facilitate exploratory activity (Smith et al., 2012; Smith and Alloway, 2014).

We recently hypothesized that the claustrum may have an active role in modulation or switching between resting state functional networks (Reser et al., 2014). These networks are defined largely by synchronous changes in blood flow (Fox and Raichle, 2007; Raichle, 2015a) or oscillations in field potentials (Srinivasan et al., 2007; Jerbi et al., 2010). Areas that form the main hubs of these networks are known to be affected in a variety of psychiatric and neurological conditions (Crossley et al., 2014; Stam, 2014). In the present study we placed neuroanatomical tracer injections in cortical areas along the cerebral midline of the common marmoset, from the medial prefrontal to the caudal anterior cingulate areas. These regions are of particular interest as they include hubs of the default mode and salience resting state functional networks (Seeley et al., 2007; Raichle, 2015b).

A key issue we have addressed is the anatomical relationship between the claustrum, adjacent anterior insular cortex, and the component areas of the salience resting state network. Neuroimaging studies have proposed that the anterior insular cortex is one of the main hubs of the salience network, implicated in the transition from task-negative to task-positive networks (Menon and Uddin, 2010). However, studies in rodents have demonstrated strong connections between the claustrum and cingulate and medial prefrontal areas (Sloniewski et al., 1986; Hoover and Vertes, 2007; Mathur et al., 2009), including those which could form a homologue of the primate salience resting state network (Goll et al., 2015; Belcher et al., 2016). Given the proximity between claustrum and insular cortex, and the relatively low resolution of the non-invasive imaging methods that are directly applicable to the human brain, it is uncertain whether the claustrum, anterior insular cortex, or both of these structures originate inputs to salience network areas. The claustrum and insular cortex are not only closely apposed (Kapakin, 2011), but also share common arterial blood supply (Marinkovic and Markovic, 1990; Ture et al., 2000; Delion and Mercier, 2014). The venous drainage of the claustrum is also shared with surrounding structures, including the internal, external, and extreme capsules, frontoparietal white matter, and striatum (Zhang et al., 2015), potentially

confounding assignment of functional activity as measured by the BOLD signal (Boubela et al., 2015). Furthermore, the claustrum is prone to partial volume artefacts in functional imaging studies (Wu et al., 2010; Hornak, 2014), as it is quite thin in cross-sectional area (Kowiański et al., 1999; Druga, 2014), and situated between two white matter tracts. It is thus critical to examine its connectivity using higher-resolution methods, in the context of the proposed functional networks.

The marmoset is an ideal model species for this study, as it is a small primate that lacks a cingulate sulcus, which simplifies injection placement. Despite the relative lissencephaly of the marmoset brain, the rostral midline region contains all of the major cytoarchitectonic divisions that have been described in Old World monkey species, such as macaques (Paxinos et al., 2012). Parcellation of the medial prefrontal and anterior cingulate regions has been well described in the marmoset (Roberts et al., 2007; Burman and Rosa, 2009; Paxinos et al., 2012). There is, in addition, significant similarity with the organization of the human medial cortex (Palomero-Gallagher et al., 2013), In particular, the transition between pregenual Area 32, which is formed by disgranular cortex, and Area 24, which is agranular, is clear in marmosets, macaques and humans, and provides a reasonable demarcation of the boundary between medial prefrontal and anterior cingulate areas.

Here we describe tracer injections placed in medial prefrontal and anterior cingulate areas of the marmoset, and describe differences in the resultant pattern of labelled neurons and axon terminals in the ipsilateral claustrum and insular cortex, in order to clarify the structural connectivity underlying known cortical hubs of the default mode and salience networks in the primate brain.

Materials and Methods:

Surgical procedures and husbandry

Tracer injection surgeries and data acquisition methods have been described in detail in previous publications (Reser et al., 2009, 2013, 2014). In this study seven tracer injections were placed along the rostral midline areas of the cerebral cortex of four adult marmosets. Case details for all animals are presented in Table 1. The tracers used were diamidino yellow (DY), cholera toxin-b subunit conjugated with gold (CTB-g**,** List Biologicals, Campbell, CA; RRID: SCR_014318) or alexa-488 (CTB-a488), and biotinylated dextran amine (BDA). All procedures were approved in advance by the Monash Animal Research Platform Animal Ethics Committee, and were in accordance with the NHMRC Australian Code of Practice for Care and Use of Animals for Scientific Purposes. All surgical procedures were performed under aseptic conditions.

Animals were premedicated with atropine and diazepam (Atrosite and Pamlin, 0.2 and 2 mg/kg, im, respectively) and anesthetized with alfaxalone (Alfaxan, 8 mg/kg, im). Peri-operative dexamethasone (0.3 mg/kg, im) and prophylactic procaine penicillin (Norocillin, 25 mg/kg, im) were administered and the animal's head was held in a stereotaxic frame. The skin overlying the cranial midline was incised and reflected, and a 0.5-1.0 cm craniotomy was opened using a dental drill. The dura mater was incised, and the resulting flaps gently reflected toward the sagittal sinus until the curvature of the dorsal midline convexity could be visualized. Small quantities of tracer were placed by pressure injection, in 50 nL steps separated by 2-5 minute intervals. The depth of each injection was determined by the stereotaxic coordinates of the target area, determined according to the Paxinos et al. atlas (generally 2.5 - 4 mm below the cortical midline; Paxinos et al., 2012), and slight back pressure was applied to the microsyringe during transit to minimize tracer leakage. After the final tracer deposit, the syringe was left in place for an additional 5 minutes to allow the material to completely exit the micropipette tip. In each surgical procedure, 4 to 5 tracer injections were placed in different areas of cortex; some of these will be reported separately as they were placed outside the area of interest, while others were excluded as they invaded the subjacent white matter. After the final injection, the dural flap was gently restored and covered with Gelfilm, and the bone fragment resulting from the craniotomy was replaced. The craniotomy seams were padded with Gelfoam, and subsequently filled with dental acrylic. After suturing the skin the animals were given replacement fluids (5 - 6 ml warmed Hartmann's solution, sc) and removed to a warm chamber for recovery. Acute post-operative analgesia was provided via buprenorphine (Temgesic, 0.01 mg/kg, im). When fully recovered and mobile, the animals were removed to a monitoring cage overnight, provided with preferred foods and fluids, and subsequently returned to

the home cage, in visual and auditory contact with other marmosets. Additional post-operative analgesia included **c**arprofen (**Carprieve,** 4 mg/kg sc) daily for 3 days following surgery.

Histology

After a recovery period of 6 - 21 days post-injection (Table 1), animals were humanely sacrificed (sodium pentobarbital, 100 mg/kg, ip) and transcardially perfused with chilled 0.1M PBS followed by 4% paraformaldehyde (PFA) in PBS. The brains were extracted, post-fixed in 4% PFA overnight, then cryoprotected in serially increasing sucrose buffer (10%-30%), blocked, and cryosectioned in the coronal plane (40 µm thickness). Adjacent sections were processed for myelin using the Gallyas silver method (Gallyas, 1979), stained for Nissl substance (using cresyl violet), mounted unstained for fluorescence microscopy, histochemically reacted for BDA using DAB enhancement, or silver enhanced for CTB-gold (see below). The total inter-section interval for each series was 200 um. After processing, sections were coverslipped using DPX medium after quick dehydration (100% ethanol) and defattening (xylene).

Myelin and Nissl series were bulk scanned at 10X magnification using an Aperio AT-2 slide scanner. The resulting images were extracted, segmented, resized, and imported into Adobe Illustrator (CS6, Adobe, Inc. San Jose, CA) using a custom workflow (scripts available on request).

BDA histochemistry: BDA was visualized using previously described methods (Reser et al., 2009). Free-floating sections were washed in 0.1 M PBS, then immersed in 0.3% H_2O_2/25% methanol for 30 min. Sections were then washed 3 times in 0.1M PBS/0.3% Triton X-100 and incubated at 4° C overnight in ABC reagent (Vectastain ABC Elite kit, Vector BioLabs, RRID:SCR_011010). At the conclusion of the ABC incubation, sections were washed for 30 min in 0.1 M PBS and reacted in diaminobenzidine with a nickel enhancer (Vectastain DAB, Vector BioLabs, RRID:SCR_011010) for 1-2 minutes. Finally, sections were rinsed twice in PBS, mounted on glass slides, dried, and coverslipped.

CTB-gold silver enhancement: Sections processed for CTb-gold were washed for 10 min in 0.1 M PBS, then mounted on slides from dH_2O containing very dilute PBS. After air drying for 2 - 7 days, tissue sections were outlined on the slides using a wax pen, then immersed briefly (30-60 sec) in dH2O and drained. In accordance with the manufacturer's protocol, several drops of silver initiator and enhancer (LI silver enhancement kit, Nanoprobes, Inc. Yaphank, NY; RRID: SCR_014319) were applied to each slide and gently agitated for 20-22 min at 20° C. The reaction was quenched in dH2O, and the slides were dried for an additional 48h before coverslipping.

Data acquisition and processing:

Fluorescent tracers: The distribution of DY and CTB-a488 was examined in unstained sections using a Zeiss Axioskop microscope (Carl Zeiss, Inc., Jena, DE). Tissue boundaries and cell locations were plotted with an X-Y stage digitizer using MD-Plot software (v. 5.2 Accustage, Shoreview, MN). Section drawings and cell positions were exported to Adobe Illustrator and overlaid with the myelin- and Nissl-stained images. Cortical and subcortical areas that contained transported label were identified based on cytoarchitectonic and myeloarchitectonic features, including those described in previous studies (Roberts et al., 2007; Burman and Rosa, 2009) and in a published atlas of the marmoset brain (Paxinos et al., 2012). Labelled cells were counted using features of Adobe Illustrator (document info: objects), and were used to generate claustrum heat maps as described below (Reser et al., 2014).

CTB-gold: The reaction product was viewed under dark field and bright field light microscopy, and cells containing clear deposits of silver were plotted and counted as described above.

BDA: Although BDA is capable of labelling retrograde projections, in this study we focused on the anterograde distribution of BDA. Occasional labelled cell bodies were observed, and in those instances, labelled somata were interpreted as positive evidence that the identified connections were reciprocal, but no attempt was made to quantify BDA label. Anterogradely labelled axon terminal fields were identified by light microscopy, and the extent of the fields was outlined using the X-Y stage digitizer and associated software. Axon terminals were differentiated from fibers of passage by the appearance of bead-like densities along the axon, transverse orientation within the tissue section, and the absence of cut ends. In contrast, fibers of passage were characterized by parallel orientation, smooth axon shafts, and the appearance of cut ends oriented into the plane of section.

Data analysis:

In addition to careful visual inspection within tissue sections, labelled cells were grouped and counted within the claustrum to produce "heat maps" showing the location of cell clusters against a lateral view of a 3-d reconstruction of this structure. Cell positions were plotted against a grid corresponding to approximately 200 X 200 uM in Adobe Illustrator CS6 (Adobe Systems, Mountain View, CA; RRID: SCR_014198), and summed cell counts were obtained for all horizontal rows in each claustrum section. This data was then exported to MatLab and aligned with the dorsal and ventral boundaries of each plotted claustrum section. The cell count array was overlaid with a color density scale representing 0 to 100% of the maximum cell count within each grid square. The resulting heatmap was smoothed with a median filter (2 pixel radius) in Adobe Photoshop CS6 (Adobe Systems, Mountain View, CA; RRID: SCR_014199), and finally overlaid on a smoothed representation of the lateral view of the claustrum, generated from the claustrum outline of each coronal section. A similar approach was used in mapping claustrum connections

from the cebus monkey (Reser et al., 2014). This approach leads to some distortion, especially with respect to the medial-lateral position of cells within the claustrum, but is informative with respect to the rostral-caudal and dorsal-ventral axes.

Photography:

Low magnification bright- and dark- field digital images of BDA and CTB-g label were obtained using a Leica DMS-1000 (Leica Microsystems, Wetzlar, DE). The resulting images were cropped and adjusted for brightness, contrast, level, and tone in Adobe Photoshop CS6 (Adobe, Inc. San Jose, CA), and arranged and labelled using Adobe Illustrator. Fluorescence photos and high magnification bright field images were captured on a Zeiss Axiocam ICC-5 camera using the Zen software suite (Carl Zeiss, Inc. Jena, DE) and similarly processed. All image adjustments were applied equally to the entire image, and occasional optical or histological artefacts in the tissue sections were retained in cropped images. Plot files, handwritten notes, and raw and processed digital images were uploaded to Lab Archives **(**Monash University edition**)** electronic notebook software (Lab Archives, Inc., Carlsbad, CA; RRID: SCR_014317). Raw scanner output files were stored to the Monash University shared server (MASSIVE). Confocal images were acquired as a series of 14 z-stacks using a Leica DMI-6000 microscope with a 63x objective. Image stacks were processed in ImageJ and exported as .png files to Adobe Illustrator for layout and labelling.

Results:

Anatomical, cytoarchitectonic, and myeloarchitectonic characteristics of the marmoset claustrum

The marmoset claustrum (Fig. 1) is a distended rhomboidal structure that occupies the subcortical space laterally adjacent to the basal forebrain and striatum. Along its rostral - caudal axis, it runs from approximately 1 mm rostral to the temporal pole to 1-2 mm rostral to the tip of the lateral sulcus. On the dorsal - ventral axis, it ranges from < 1mm thick at its rostral end, spreading to an approximately 7mm long sinuous band of gray matter at the level of the anterior commissure, and tapering to a shortened 2mm long oval at its caudal end. A prominent feature of the marmoset claustrum, as seen in coronal sections, is the approximately 90^{o} shift in orientation of the long axis of the nucleus, which occurs at a level approximately coincident with the temporal pole. This deviation results in ambiguity when standard anatomical terms of reference are applied (e.g. dorsal-ventral; medial-lateral) without further qualification. To alleviate this problem, in the remainder of this report, locations in the claustrum will be described first by an indication of rostral-caudal position, followed by the medial-lateral or dorsal-ventral locator. Thus, we will refer to the rostral claustrum as the portion located anterior to the optic chiasm (A-P +11.0; Paxinos et al., 2012), in which the claustrum gradually assumes oblique and horizontal profiles in cross-section. The middle segment of the claustrum extends from A-P +11.0 to approximately the posterior end of the anterior commissure (A-P +8.0), where a near-vertical cross section profile is most obvious, and the caudal segment extends from this point to the caudal terminus of the claustrum (A-P +6.5). This segmentation is framed in terms of landmark anatomical structures as a convenience for descriptive purposes, and we emphasize that no functional significance is attributed to these terms.

The claustrum is very lightly myelinated along its entire rostral-caudal extent, in strong contrast to the adjacent external and extreme capsule white matter tracts. On this basis, myelin staining is a reliable marker for delineation of the claustrum boundaries (Fig. 1, lower right panel). However, separation of claustrum from adjacent structures is difficult at the rostral terminus, where the claustrum merges with the caudal orbital cortex, and at the fundus of the lateral sulcus, where the extreme capsule deviates into the temporal lobe.

Neuroanatomical tracer injections

Successful tracer injections were defined by a clearly visible core located away from the underlying white matter, with transport of label to distant targets, including the thalamus or contralateral homotopic cortex. Four injections were located completely or mostly within areas 32 and 32V, while three injections were localized to subdivisions of area 24 (Fig. 2). Full descriptions of cortico-cortical and thalamo-cortical connectivity for each injection will be published separately.

Areas 32 and 32V

Area 32 in the marmoset is well-defined based on cytoarchitectural characteristics, including: a diffuse layer 4; well-defined layer 5a with darkly staining neurons; and a gradient of cell sizes from top to bottom of layer 3 (Burman and Rosa, 2009). It occupies a large portion of the medial surface of the marmoset frontal pole, being bounded dorsally by area 9, rostrally by area 10, caudally by areas 24 and 25, and ventrally by a distinct band of cortex which has as its main feature a darker myelination relative to adjacent cortex, particularly at the level of the outer band of Baillarger. This band was originally referred to as area 10mc, following the nomenclature initially proposed by Saleem et al. (2008) for the macaque. However, a subsequent study using a wider range of neurochemical markers indicated that it shares many features with area 32, prompting a change in nomenclature (area 32 ventral, or 32V; Paxinos et al., 2012).

Three injections (Cases CJ155-CTBa488, CJ155-CTBg and CJ148 BDA) were placed in area 32. The resulting pattern of label in the claustrum and insular cortex is illustrated in Figures 3-5. Following injection of CTBalexa488 into A32, retrogradely labelled cell bodies were evident throughout the rostral and middle segments of the claustrum, with 2 especially dense patches located in the mid-dorsal (at approximately the dorsal-ventral level of the anterior commissure) and ventrolateral parts of the claustrum, as shown in the heat map in the lower right panel of Figure 3. Additional labelled neurons were present throughout the rostral 1/3 of the claustrum (Fig. 3A-D). Only a few isolated cells were evident in the caudal 1/2 of the claustrum (Fig. 3 E-H). In the insular cortex, a dense patch of labelled cells was observed in the orbital proisocortex (area OPro), with less dense label evident in the adjacent orbital periallocortex (OPAl) and gustatory cortex (Gu) areas (Fig. 3 A-B). In contrast, negligible retrograde label was observed in the classically defined agranular, disgranular or granular insular areas (Fig. 3 C-H). The distribution of labelled neurons in both the claustrum and orbital proinsular areas OPAl and OPro was remarkably consistent, as shown in Fig. 4, which depicts the pattern of label resulting from injection of CTB-g into A32 of the opposite hemisphere of case CJ155. Note in particular the dense label in OPAl and OPro, which was coextensive with patches of labelled claustrum neurons (Fig. 4 A), and the absence of label along the remaining anterior-posterior extent of the insula (Fig. 4 B-H).

Anterograde label in the claustrum-insula region following A32 injection (case CJ148-BDA; Fig. 5 A-C) showed a roughly similar distribution to the retrograde label, with the densest terminal label in the rostral and mid claustrum (Fig. 5 G-I), and negligible axon terminals in the caudal claustrum (Fig. 5 J-L). In the insular cortex, there was a dense patch of terminal label in are OPro, with lighter terminals evident in the medially adjacent area OPAl, and in the laterally adjacent area Gu (Fig. 5 D-F). No retrogradely labelled cell bodies were observed in the pro-insular areas following this

injection, and sparse label was evident in the classical agranular insular area (Fig. 5 H-I). No terminal label was evident in the disgranular or granular insula (Fig 5. K-L).

Two injections were primarily located within A32V (case CJ132-DY and case CJ148-DY). In both of those injections, the distribution of labelled neurons in the claustrum was more restricted than the A32 case described above, but the areas of densest label were consistent with the pattern of A32 label; i.e., cell clusters were localized to the mid and ventral-lateral areas (Figs. 6 A-E; 7 A-E), and the caudal and dorsal claustrum exhibited very little connectivity with A32V or A32 (Figs. 6 F-H; 7 F-J). In both A32V injections, a patch of labelled neurons was observed in OPAl and OPro, with no label (Case CJ148-DY; Fig 6 A-J) or only 1- 2 isolated cells (case CJ132-DY; Fig. 7 A-H) evident in the agranular, disgranular or granular subdivisions of the insula. Note that several of these cells may have been so-called "shell neurons" (see below), and could not readily be assigned to the claustrum or to the deep layers of insular cortex (Fig. 7 E-H).

Area 24

Area 24 in the marmoset includes four cytoarchitectural subdivisions (areas 24a-d; Paxinos et al., 2012). They are formed by agranular cortex, with the density of myelination increasing gradually from ventral (area 24a, located adjacent to the genu of the corpus callosum) to dorsal (area 24d). Where possible, we also identified the subdivisions where injections were placed. However, in some cases, this was not feasible, due to the relatively small dorsal - ventral extent of the targeted areas and the local disruption of cytoarchitectonic features resulting from the fluid volume of the injection. Two injections were confined within subdivisions of area 24 (case CJ157-CTBg and case CJ157-BDA). Injections into A24 exhibited the densest thalamic label in subdivisions of the ventral anterior nucleus (VA), in contrast to the dense MD input observed following injections in A32V (Fig. 8).

A retrograde tracer injection centred in the rostral portion of A24b (case CJ157-CTBg) resulted in an expanse of labelled claustrum neurons which overlapped the "hot spots" of label observed after injections in A32, but extended more dorsally, especially in the mid-claustrum (Fig. 9 A-D). Furthermore, labelled claustrum neurons were observed in the dorsal claustrum along its entire rostral-caudal extent (Fig. 9 E-G and heatmap in lower right panel), with no labelled cells in the ventral portion of the claustrum. This pattern is markedly different from the distribution of transported label following the A32 and A32V injections described above (Figs. 3-6, heatmaps).

In the insular region, the distribution of labelled cells was shifted caudally relative to the A32/32V injections, and numerous labelled soma were present in the classical insula, especially in the disgranular and granular subdivisions (Fig. 9 C-G). Negligible label was evident in the orbital proinsular areas OPAl and OPro, though a dense patch of cells was present in the nearby proisocortical motor region (ProM; Fig. 9 A-C).

The BDA injection in caudal A24 (case CJ157-BDA; Fig. 10 A-B) represented the most caudal injection included in this series of experiments, and showed almost no claustrum label (Fig. 10 C). In contrast, this injection produced a dense and specific band of terminal label in the insula, especially in the granular and disgranular subdivisions (Fig. 10 D-L). No terminal label was observed in the orbital proinsular areas or rostral-mid claustrum following this injection, despite clear evidence that transport of the BDA tracer was sufficient to identify monosynaptic projections in those areas had they been present, e.g. label was observed in the adjacent striatum.

"Shell" neurons

Consistent with reports from immunohistochemical and cytoarchitectonic studies in rodents (Mathur et al., 2009), monkeys (Miyashita et al., 2005; Reser et al., 2014), and humans (Pirone et al., 2012) we observed scattered retrogradely labelled neurons outside the apparent boundary of claustrum gray matter (Figure 11 A-B). These “shell” neurons were most commonly observed in the extreme capsule following injections in area 24, and could not be conclusively assigned to either the claustrum or adjacent deep layers of the insular cortex. For purposes of cell counting, shell neurons were assigned to the claustrum, but in practice, there were not enough of them to affect the heat map distributions. A few shell neurons were observed in the external capsule, but they were more common in the extreme capsule and in the white matter at the ventrolateral extreme of the claustrum (e.g. Fig. 5 D-E). In those cases where shell neurons were present, they were generally found at the same rostral-caudal and dorsal-ventral levels as prominent patches of labelled claustrum neurons, i.e. isolated shell neurons were rare.

Interhemispheric projections

In all cases, isolated labelled cell bodies were observed in the contralateral claustrum, and contralateral anterograde terminal label was present in the BDA-injected animals. However, contralateral label was invariably much lighter than the ipsilateral, in most cases amounting to only a few cells or labelled terminals along the entire rostral-caudal length of the claustrum. In these instances, the contralateral labelled neurons were in the same general location within the claustrum as the ipsilateral labelled cells and terminals.

Discussion:

Homology of marmoset medial prefrontal and anterior cingulate cortex with macaque and human

The anterior cingulate cortex is identified as a site of activation in blood flow-dependent functional studies across a wide array of cognitive tasks and emotional states, and often exhibits disruptions in various acute and chronic neuropsychological conditions. While the region has been examined in functional imaging studies, there is often ambiguity in these studies regarding the precise anatomical location of active voxels. In studies of non-human primates, it is generally the case that the anterior cingulate region consists of the rostral and dorsal portion of area 24, the subgenual portion of area 25, and at least the caudal portion of Area 32. The boundary between area 32 and area 24 is cytoarchitectonically well-defined, in all primates, as a transition from disgranular to agranular cortex (Vogt et al., 2013). Importantly, Vogt and colleagues have identified at least 2 subdivisions of A32 in the human (32' and d32; Vogt et al., 2013) which are not evident in macaques or other non-human primate species, and their differentiation between primate A32 and A24 is in part based on cortico-cortical connectivity, especially with the posterior cingulate and retrosplenial areas. The differential connectivity with the insula-claustrum region which we report here is largely consistent with Vogt and colleagues' parcellation of A32 and A24 in the macaque.

The principal thalamic input to area 32 originates in the medial dorsal nucleus of the thalamus (MD), which is typically a characteristic of prefrontal cortical areas (Fuster, 2008; Burman et al., 2011). In contrast, injections into A24 resulted in more diffuse thalamic label, centered principally in the ventral anterior and ventral antero-medial nuclei (VA and VAM, respectively).

MD is a large thalamic nucleus with outputs to the entire prefrontal cortex, among numerous other connections (reviewed in Mitchell and Leopold, 2015), and it is comprised of multiple subdivisions in marmosets (Paxinos et al., 2012). The labelled MD neurons in this sample were not clearly restricted to a particular subdivision of MD, and it is therefore difficult to attribute functional significance to the observed MD projections. This is compounded by the relative paucity of functional information about the potential interaction of thalamocortical circuits with the claustrum, although direct connections between the claustrum and MD have been reported in the macaque (Erickson et al., 2004) and other species (Carey and Neal, 1986; Gritti et al., 1987). We therefore regard the differential pattern of thalamic connectivity reported here more as an supporting evidence for anatomical segregation of A24 and A32, rather than inferring functional significance. This pattern of connectivity, in conjunction with the aforementioned cytoarchitectonic and myeloarchitectonic differences, is consistent with classification of A32 as a component of MPFC, and A24 as a major component of the dorsal anterior cingulate cortex.

With respect to our hypothesis that the claustrum may have a role in modulating the asynchrony of cortical functional networks (Reser et al., 2014; Patru and Reser, 2015b) a key focus of future studies will be to assess whether the separation of A32 and A24 based on anatomy and clasutrum-insula connectivity that we report here is accompanied by changes in functional connectivity, especially in the salience and default mode networks. Both of these networks have been identified in the marmoset (Belcher et al., 2013, 2016), and their findings included functional connectivity between the anterior cingulate and the insula-claustrum region (Belcher et al., 2016). The possibility and implications of co-activation of the claustrum and anterior insula is discussed below.

Topography of claustrum-insular projections

A clear rostral-caudal gradient of transported label was evident across injections in this study. In particular, injections into the rostral anterior cingulate and medial prefrontal cortex yielded claustrum label in a band extending from the rostral most claustrum sections along the ventral axis of the claustrum, with a consistent second patch of labelled neurons in the caudal and ventral aspect of the claustrum. In contrast, as the injections moved caudally along the midline, claustrum label shifted dorsally, with the caudal-most injection producing a broad expanse of labelled cells along the entire length of the dorsal claustrum. Previous studies in primates (Pearson et al., 1982) have shown that the dorsal claustrum has a high density of somatomotor projections, which would be consistent with the interpretation that the caudal-most retrograde tracer injection in this study (CJ157-CTBg) was located in what has previously been termed the mid-cingulate or motor cingulate cortex.

The rostral-caudal gradient was also evident in the insular and peri-insular connections resulting from our injections. Injections into A32 and rostral A24 resulted in deposition of tracer in cortical areas rostral to the temporal pole, including regions previously classed as anterior insula (see below). Negligible label was evident in the agranular, disgranular, or granular insula following these injections, despite clear evidence that label was transported to other brain regions equally far away or further away from the injection site, including inferior temporal and retrosplenial areas of cortex (full details of cortico-cortical connections arising from these injections will be published separately). In contrast, injections placed more caudally in A24 showed dense and well-bounded patches of label in the classical insular areas, with negligible connections to rostral insular and peri-insular areas or the claustrum. The most caudal injection in this study (CJ157-BDA) resulted in only a few isolated axon terminals in the entire claustrum, but a prominent and specific connection with disgranular and agranular insula. Overall, this pattern suggests that the monosynaptic connectivity of the caudal portion of the anterior cingulate cortex in the marmoset is preferentially connected with the classical insula, while the peri-genual portion of the anterior cingulate has connections with the rostral and ventral claustrum, as well as the orbital proinsular areas. In this and

our previous studies of claustrum projections to the cerebral cortex of New World monkeys (Burman et al., 2011; Reser et al., 2014), there was little evidence of strong interhemispheric claustro-cortical connections such as those observed in rodent (Smith et al., 2012; Smith and Alloway, 2014; Watson et al., 2016). Our data are more consistent with the pattern reported in the cat (Squatrito et al., 1980; Macchi et al., 1983; Markowitsch et al., 1984), with only light or moderate contralateral label reported in those studies. This does not preclude the possibility of strong interhemispheric projections between the two claustrums, which would be undetectable to monosynaptic tracers injected into cortical targets, but it does suggest that the whatever interhemispheric communication occurs in the claustro-cortical circuit would be via a polysynaptic, and presumably slower-conducting, neural pathway than the ipsilateral component of the circuit. Direct claustrum-claustrum connectivity has been reported in diffusion-weighted imaging studies in humans (Milardi et al., 2013).

Nomenclature of "anterior insula" areas

The classical agranular, disgranular, and granular subdivisions of the primate insula are all located on the medial bank of the lateral sulcus, and bounded dorsally by the superior limiting sulcus. In humans, the agranular insula extends beyond the rostral limit of the lateral sulcus, reaching the caudal boundary of the orbit (Ongur et al., 2003; Craig, 2009; Gallay et al., 2012; Christopher et al., 2014), and Craig (2009) has suggested that this region has no homologue in non-human primates. In past studies of the marmoset, an orbital area extending rostrally from the limit of the lateral sulcus has been identified as anterior insular cortex (Roberts et al., 2007; Burman and Rosa, 2009; Hardman and Ashwell, 2012). However, in the stereotaxic atlas of Paxinos et al., (2012), this region was reclassified as orbital periallocortex (OPAI) and orbital proisocortex (OPro), with the rostral limit of the agranular insula extending only to the rostral-caudal level of the optic chiasm. Full resolution of the cytoarchitecture and homology of these areas will require more detailed investigation across model species, and possibly of human tissue samples. However, connectivity between the medial prefrontal and anterior cingulate areas of the macaque (Carmichael and Price, 1994; Ongur and Price, 2000) and our findings in the marmoset are consistent with OPAI and OPro areas, rather than the classically defined insular cortex (i.e., agranular, disgranular, and granular divisions), containing the likely homologues of anterior insula to cingulate/medial prefrontal cortex connections seen in the human. We therefore suggest that the "anterior insula" as described in imaging studies may include the orbital periallo- and proisocortical areas of the marmoset (i.e. these regions may homologous with the rostral agranular insula observed in macaques and humans). Apart from the nomenclature of insular and peri-insular regions, the frequent co-occurrence of transported label in these areas and the antero-ventral claustrum following injections in A32 and rostral A24 in our study suggests that information processing in the

primate salience network is likely to include substantial activation of the claustrum. Our findings are interesting in light of the suggestion by Mathur and colleagues (2009)that the rostral claustrum and insular cortex are a single entity in the rodent, as these data suggest that the anterior insula-claustrum region may have undergone some phylogenetic modification, with somewhat better resolution of the areas by cytoarchitecture, but retention of a close relationship with respect to cingulate connectivity. Obviously, functional studies will be necessary to resolve what differences may exist between the rostral- and mid- claustrum and the anterior insular cortex, but as suggested above, imaging is unlikely to provide a conclusive result. Given the close apposition of the claustrum and insula, as well as the commonality of blood supply to this region, our data suggest that resolution of claustrum vs. insular origins of activated voxels in functional imaging studies may not be straightforward.

Potential for claustrum misassignment in clinical imaging and lesion studies

Our data clearly show the need for closer attention to anatomical parcellation of the insular cortex-claustrum-lateral striatum region, both in animal studies, and in examinations of human functional imaging and clinical pathology. The close apposition of the claustrum with insular cortex and the putamen in primates has been well described (Kapakin, 2011), but it bears repeating that it is possible to traverse the insular cortex, extreme capsule, dorsal claustrum, and lateral putamen along a linear path of only a few millimeters from the bank of the lateral sulcus, even in the human brain. Furthermore, and potentially even more problematic from the point of view of functional studies, is the commonality of blood supply and venous return between these structures. Surgically, the arteries and arterioles which supply the claustrum also supply the insular cortex and extreme capsule (Delion and Mercier, 2014). Recently, the principal venous drainage of the claustrum, extreme and external capsules, putamen, and frontoparietal white matter has been shown to be via the thalamostriate vein complex (Zhang et al., 2015). In that study, the authors noted that MRI signal changes in the claustrum associated with fever-induced status epilepticus had likely been misidentified as either extreme capsule or insular hyperintensity. Thus, shared vascularization has significant implications for assignment of functional activity in studies of regional blood flow and oxygenation in the insula- claustrum region.

Boubela and colleagues (2015) showed by susceptibility-weighted imaging that functional MRI activity evoked during a face recognition task, which had previously been attributed to the amygdala, was likely to have been partly or completely an artefact of venous drainage via the basal vein of Rosenthal (BVR). In that study, the most likely source of the measured activity was the fusiform area, quite distant from the amygdala, but which also drains via the BVR. In their discussion of the wider implications of this interesting finding, the authors of that study specifically implicated the insula as a brain area subject to large-vessel artefacts (Boubela et al., 2015). In our

view, these findings highlight the need for detailed understating of the structural anatomy and connectivity of this region in order to make and test hypotheses regarding claustrum function, and the data from this study suggest that it would be easy to misallocate activity to the insula which is partially or completely generated in the adjacent claustrum. An alternate possibility is that imaging results attributed to the anterior insula reflect co-activation of the insula and claustrum, and these structures may comprise a functional unit in some circumstances. Monosynaptic connections between the claustrum and insula are negligible or very light in the cat (Markowitsch et al., 1984), suggesting that there is relatively little modulation of the claustrum by the insula, or vice-versa. However, co-activation of the claustrum and insula has been reported for voluntary suppression of blinking (Lerner et al., 2009), and interestingly, anterior cingulate was also activated in this task, so distal modulation of both regions is possible. The advent of higher field strength imaging, along with other methods of investigating activity in the claustrum-insula region (Koubeissi et al., 2014), may help to clarify when and whether the claustrum and insula act separately or in concert.

A final consideration for understanding functional activation of this region will be understanding the nature and role of "shell neurons", and whether these cells are part of the claustrum, insula, or both. Numerically, labelled neurons in the extreme capsule did not represent a large segment of the labelled cell population, and they were localized to the same dorsal-ventral level as the main clusters of retrogradely labelled claustrum neurons, but it is conceivable that these cells represent a functionally distinct population. Exploration of this question will likely require high precision methods for labelling and recording from specific cells, and most such techniques are not currently available in primate species.

"Shell neurons" may confound identification of the claustrum-insula boundary

So-called shell neurons, or cells which exist outside the histologically apparent boundaries of the claustrum, have been reported in rodents (Mathur et al., 2009) and in macaque monkeys (Miyashita et al., 2005) following histological studies, and a subset of these neurons were shown to project to cortical targets in motor, extrastriate visual, and polymodal association areas of cortex (Miyashita, et al., 2005). Here we confirm the existence of neurons in the extreme capsule that project to cortex in New World monkeys, and extend the cortical distribution of these neurons to include the anterior cingulate region. While the functional significance of these neurons is unclear, discontinuities or cellular "islands" in the claustrums of large-brained species have been interpreted as counter-evidence against hypothesized claustrum functions which rely on intrinsic claustrum connectivity or the existence of a gap-junction based claustral syncytium (Baizer, 2014). While the claustrum in marmosets appears less fragmented than that of the macaque or human, especially in the mid-ventral region, our data indicate: 1) there is some discontinuity in cell populations within the marmoset claustrum; and 2) cells in the discontinuous regions project to cortical targets. Definitive

classification of shell neurons will likely require use of molecular techniques for identification, and until such information is available, it will remain uncertain whether these cells are components of the insula, claustrum, or both.

Implications for network hypotheses of claustrum function

Several recent hypotheses for claustrum function revolve around the highly networked connectivity of the claustrum, which has been demonstrated in humans (Torgerson and Van Horn, 2014) and rodents (Bota et al., 2015). Based upon the claustrum connectivity of prefrontal cortex in the cebus monkey, we recently proposed a novel hypothesis which suggests that the claustrum may play a role in switching between synchrony of task negative and task positive networks, such as the default mode and central executive or dorsal attention networks (Reser et al., 2014). Such a role has previously been suggested for the salience network (Menon and Uddin, 2010), which was first described in human imaging studies by Seeley and colleagues (2007), and has subsequently been reported in marmosets (Belcher et al., 2013). The critical axis of the salience network in functional imaging studies appears to be the connectivity between the anterior cingulate region and the insula, in particular the anterior insula (Seeley et al., 2007). However, close examination of the data provided in previous descriptions of the salience network strongly suggests that activity in the "insular" portion of this axis extends to the claustrum and surrounding white matter. Overlap with the claustrum is also observed in studies of disrupted salience in bipolar disorder (Radaelli et al., 2014) and delusional parasitosis (Wolf et al., 2013), though in both of those studies, the reports focused solely on activity in the insula. It is clear from our data that the pattern of structural connectivity in the insula-claustrum region is consistent with a claustrum origin for some or all of this activity.

Acknowledgements

The authors gratefully acknowledge the assistance of Ms. Maree Reser for proofreading and editing of this manuscript. We also thank Dr. Judy Callaghan of the Monash Microimaging Platform, who provided expert assistance with the confocal microscopy images in Figure 11. This work was supported by NHMRC Project Grant 10468140 (DHR). Portions of this work were presented at the 2015 Annual Meeting of the Society for Neuroscience (Reser, et al. Comparative Anatomy and Evolution Nanosymposium presentation 563.06, 11/20/2015).

Conflict of interest statement

The authors declare they have no competing financial interests.

Role of authors:

All authors had full access to all the data in the study and take responsibility for the integrity of the data and the accuracy of the data analysis.

DHR: Conceived, designed, and interpreted study; performed tracer injections; collected and analyzed electronic data; reconstructed anatomical specimens; wrote and edited manuscript.

PM, JC, MDMQ: Wrote computer code; managed electronic data, created heatmap figures.

SS, KW, KW: Executed histological staining, plotted fluorescence and BDA tracers, provided surgical assistance and post-operative care, managed electronic data.

MGPR: Oversaw project execution and data interpretation, co-wrote and edited manuscript.

Literature cited

Baizer J. 2014. The Structure and Connections of the Claustrum: The Neurochemical Organization of the Claustrum. In: Smythies J, Edelstein L, Ramachandran V, editors. The Claustrum: Structural, Functional, and Clinical Neuroscience. . San Diego, CA: Academic Press (Elsevier).

Belcher AM, Yen CC, Stepp H, Gu H, Lu H, Yang Y, Silva AC, Stein EA. 2013. Large-scale brain networks in the awake, truly resting marmoset monkey. J Neurosci [Internet] 33:16796–16804. Available from: http://www.ncbi.nlm.nih.gov/pubmed/24133280

Belcher AM, Yen CC-C, Notardonato L, Ross TJ, Volkow ND, Yang Y, Stein EA, Silva AC, Tomasi D. 2016. Functional Connectivity Hubs and Networks in the Awake Marmoset Brain. Front Integr Neurosci 10:9.

Bota M, Sporns O, Swanson LW. 2015. Architecture of the cerebral cortical association connectome underlying cognition. Proc Natl Acad Sci U S A [Internet] 112:E2093–101. Available from: http://www.ncbi.nlm.nih.gov/pubmed/25848037

Boubela RN, Kalcher K, Huf W, Seidel EM, Derntl B, Pezawas L, Nasel C, Moser E. 2015. fMRI measurements of amygdala activation are confounded by stimulus correlated signal fluctuation in nearby veins draining distant brain regions. Sci Rep [Internet] 5:10499. Available from: http://www.ncbi.nlm.nih.gov/pubmed/25994551

Burman KJ, Reser DH, Richardson KE, Gaulke H, Worthy KH, Rosa MG. 2011. Subcortical projections to the frontal pole in the marmoset monkey. Eur J Neurosci [Internet] 34:303–319. Available from: http://www.ncbi.nlm.nih.gov/pubmed/21714814

Burman KJ, Rosa MG. 2009. Architectural subdivisions of medial and orbital frontal cortices in the marmoset monkey (Callithrix jacchus). J Comp Neurol [Internet] 514:11–29. Available from: http://www.ncbi.nlm.nih.gov/pubmed/19260047

Carey RG, Neal TL. 1986. Reciprocal connections between the claustrum and visual thalamus in the tree shrew (Tupaia glis). Brain Res 386:155–168.

Carmichael ST, Price JL. 1994. Architectonic subdivision of the orbital and medial prefrontal cortex in the macaque monkey. J Comp Neurol [Internet] 346:366–402. Available from: http://www.ncbi.nlm.nih.gov/pubmed/7527805

Christopher L, Koshimori Y, Lang AE, Criaud M, Strafella AP. 2014. Uncovering the role of the insula in non-motor symptoms of Parkinson's disease. Brain 137:2143–2154.

Craig ADB. 2009. How do you feel--now? The anterior insula and human awareness. Nat Rev Neurosci 10:59–70.

Crossley NA, Mechelli A, Scott J, Carletti F, Fox PT, McGuire P, Bullmore ET. 2014. The hubs of the human connectome are generally implicated in the anatomy of brain disorders. Brain [Internet] 137:2382–2395. Available from: http://www.ncbi.nlm.nih.gov/pubmed/25057133

Delion M, Mercier P. 2014. Microanatomical study of the insular perforating arteries. Acta Neurochir [Internet] 156:1991–1998. Available from: http://www.ncbi.nlm.nih.gov/pubmed/24986536

Druga R. 2014. The structure and connections of the claustrum. In: Smythies J, Edelstein L, Ramachandran V, editors. The Claustrum: Structural, Functional, and Clinical Neuroscience. San Diego, CA: Academic Press (Elsevier, Inc.). p 29–84.

Erickson SL, Melchitzky DS, Lewis DA. 2004. Subcortical afferents to the lateral mediodorsal thalamus in cynomolgus monkeys. Neuroscience 129:675–690.

Fox MD, Raichle ME. 2007. Spontaneous fluctuations in brain activity observed with functional magnetic resonance imaging. Nat Rev Neurosci [Internet] 8:700–711. Available from: http://www.ncbi.nlm.nih.gov/pubmed/17704812

Fuster JM. 2008. The Prefrontal Cortex (Fourth-Edition).

Gallay DS, Gallay MN, Jeanmonod D, Rouiller EM, Morel A. 2012. The insula of Reil revisited: multiarchitectonic organization in macaque monkeys. Cereb Cortex [Internet] 22:175–190. Available from: http://www.ncbi.nlm.nih.gov/pubmed/21613468

Gallyas F. 1979. Silver staining of myelin by means of physical development. Neurol Res [Internet] 1:203–209. Available from: http://www.ncbi.nlm.nih.gov/pubmed/95356

Goll Y, Atlan G, Citri A. 2015. Attention: the claustrum. Trends Neurosci [Internet]. Available from: http://www.ncbi.nlm.nih.gov/pubmed/26116988

Gritti I, Mariotti M, Mancia M. 1987. Limbic and brainstem afferents to thalamic mediodorsal nucleus: a horseradish peroxidase study. Neurosci Lett 76:345–350.

Hardman CD, Ashwell KWS. 2012. Stereotaxic and Chemoarchitectural Atlas of the Brain of the Common Marmoset (Callithrix jacchus). Taylor & Francis. Available from: https://books.google.com.au/books?id=-3wA7bfLPs0C

Hoover WB, Vertes RP. 2007. Anatomical analysis of afferent projections to the medial prefrontal cortex in the rat. Brain Struct Funct [Internet] 212:149–179. Available from: http://www.ncbi.nlm.nih.gov/pubmed/17717690

Hornak J. 2014. The Basics of MRI. Available from: https://www.cis.rit.edu/htbooks/mri/inside.htm

Jerbi K, Vidal JR, Ossandon T, Dalal SS, Jung J, Hoffmann D, Minotti L, Bertrand O, Kahane P, Lachaux JP. 2010. Exploring the electrophysiological correlates of the default-mode network with intracerebral EEG. Front Syst Neurosci [Internet] 4:27. Available from: http://www.ncbi.nlm.nih.gov/pubmed/20661461

Kapakin S. 2011. The claustrum: three-dimensional reconstruction, photorealistic imaging, and stereotactic approach. Folia Morphol (Warsz) [Internet] 70:228–234. Available from: http://www.ncbi.nlm.nih.gov/pubmed/22117238

Koubeissi MZ, Bartolomei F, Beltagy A, Picard F. 2014. Electrical stimulation of a small brain area reversibly disrupts consciousness. Epilepsy Behav [Internet] 37:32–35. Available from: http://www.ncbi.nlm.nih.gov/pubmed/24967698

Kowiański P, Dziewiatkowski J, Kowiańska J, Moryś J, Kowianski P, Dziewiatkowski J, Kowianska J, Morys J. 1999. Comparative anatomy of the claustrum in selected species: A morphometric analysis. Brain Behav Evol [Internet] 53:44–54. Available from: http://www.ncbi.nlm.nih.gov/pubmed/9858804

Lerner A, Bagic A, Hanakawa T, Boudreau EA, Pagan F, Mari Z, Bara-Jimenez W, Aksu M, Sato S, Murphy DL, Hallett M. 2009. Involvement of insula and cingulate cortices in control and suppression of natural urges. Cereb Cortex 19:218–223.

Macchi G, Bentivoglio M, Minciacchi D, Molinari M. 1983. Claustroneocortical projections studied in the cat by means of multiple retrograde fluorescent tracing. J Comp Neurol [Internet] 215:121–134. Available from: http://www.ncbi.nlm.nih.gov/pubmed/6853768

Marinkovic R, Markovic L. 1990. [Vascularization of the insular cortex and claustrum in human development]. Srp Arh Celok Lek [Internet] 118:17–21. Available from: http://www.ncbi.nlm.nih.gov/pubmed/2218728

Markowitsch H, Irle E, Bang-Olsen R, Flint-Egebak P. 1984. Claustral efferents to the cat's limbic cortex studied with retrograde and anterograde tracing techniques. Neuroscience 12:409–425.

Mathur BN, Caprioli RM, Deutch AY. 2009. Proteomic analysis illuminates a novel structural definition of the claustrum and insula. Cereb Cortex [Internet] 19:2372–2379. Available from: http://www.ncbi.nlm.nih.gov/pubmed/19168664

Menon V, Uddin LQ. 2010. Saliency, switching, attention and control: a network model of insula function. Brain Struct Funct [Internet] 214:655–667. Available from: http://www.ncbi.nlm.nih.gov/pubmed/20512370

Milardi D, Bramanti P, Milazzo C, Finocchio G, Arrigo A, Santoro G, Trimarchi F, Quartarone A, Anastasi G, Gaeta M. 2013. Cortical and subcortical connections of the human claustrum revealed in vivo by constrained spherical deconvolution tractography. Cereb Cortex [Internet] 25:406–414. Available from: http://www.ncbi.nlm.nih.gov/pubmed/24014669

Mitchell JF, Leopold DA. 2015. The marmoset monkey as a model for visual neuroscience. Neurosci Res [Internet] 93:20–46. Available from: http://www.scopus.com/record/display.url?origin=citedby&eid=2-s2.0-84927913318&citeCnt=106&noHighlight=false&sort=plf-f&cite=2-s2.0-0026564702&src=s&imp=t&sid=A4715EBF0F93DB3D52BF952E37CE78DC.fM4vPBipdL1BpirDq5Cw%3a20&sot=cite&sdt=a&sl=0&relpos=2

Miyashita T, Nishimura-Akiyoshi S, Itohara S, Rockland KS. 2005. Strong expression of NETRIN-

G2 in the monkey claustrum. Neuroscience [Internet] 136:487–496. Available from: http://www.ncbi.nlm.nih.gov/pubmed/16203099

Ongur D, Ferry AT, Price JL. 2003. Architectonic subdivision of the human orbital and medial prefrontal cortex. J Comp Neurol [Internet] 460:425–449. Available from: http://www.ncbi.nlm.nih.gov/pubmed/12692859

Ongur D, Price JL. 2000. The organization of networks within the orbital and medial prefrontal cortex of rats, monkeys and humans. Cereb Cortex 10:206–219.

Palomero-Gallagher N, Zilles K, Schleicher A, Vogt BA. 2013. Cyto- and receptor architecture of area 32 in human and macaque brains. J Comp Neurol [Internet] 521:3272–3286. Available from: http://www.ncbi.nlm.nih.gov/pubmed/23787873

Patru MC, Reser DH. 2015a. A New Perspective on Delusional States□-□Evidence for Claustrum Involvement. Front psychiatry [Internet] 6:158. Available from: http://www.pubmedcentral.nih.gov/articlerender.fcgi?artid=4639708&tool=pmcentrez&rendertype=abstract

Patru MC, Reser DH. 2015b. A New Perspective on Delusional States□-□Evidence for Claustrum Involvement. Front psychiatry 6:158.

Paxinos G, Watson C, Petrides M, Rosa M, Tokuno H. 2012. The Marmoset Brain in Stereotaxic Coordinates. London: Academic Press, Elsevier.

Pearson RC, Brodal P, Gatter KC, Powell TP. 1982. The organization of the connections between the cortex and the claustrum in the monkey. Brain Res [Internet] 234:435–441. Available from: http://www.ncbi.nlm.nih.gov/pubmed/6800568

Radaelli D, Poletti S, Gorni I, Locatelli C, Smeraldi E, Colombo C, Benedetti F. 2014. Neural correlates of delusion in bipolar depression. Psychiatry Res [Internet] 221:1–5. Available from: http://www.ncbi.nlm.nih.gov/pubmed/24200366

Raichle ME. 2015a. The Brain's Default Mode Network. Annu Rev Neurosci [Internet] 38:433–447. Available from: http://dx.doi.org/10.1146/annurev-neuro-071013-014030

Raichle ME. 2015b. The Brain's Default Mode Network. Annu Rev Neurosci 38:433–447.

Remedios R, Logothetis NK, Kayser C. 2014. A role of the claustrum in auditory scene analysis by reflecting sensory change. Front Syst Neurosci [Internet] 8:44. Available from: http://www.ncbi.nlm.nih.gov/pubmed/24772069

Reser DH, Burman KJ, Richardson KE, Spitzer MW, Rosa MGP. 2009. Connections of the marmoset rostrotemporal auditory area: express pathways for analysis of affective content in hearing. Eur J Neurosci [Internet] 30:578–592. Available from: http://www.ncbi.nlm.nih.gov/pubmed/19663937

Reser DH, Burman KJ, Yu HH, Chaplin TA, Richardson KE, Worthy KH, Rosa MG. 2013. Contrasting patterns of cortical input to architectural subdivisions of the area 8 complex: a retrograde tracing study in marmoset monkeys. Cereb Cortex [Internet] 23:1901–1922. Available from: http://www.ncbi.nlm.nih.gov/pubmed/22735155

Reser DH, Richardson KE, Montibeller MO, Zhao S, Chan JM, Soares JG, Chaplin TA, Gattass R, Rosa MG. 2014. Claustrum projections to prefrontal cortex in the capuchin monkey (Cebus apella). Front Syst Neurosci [Internet] 8:123. Available from: http://www.ncbi.nlm.nih.gov/pubmed/25071475

Roberts AC, Tomic DL, Parkinson CH, Roeling TA, Cutter DJ, Robbins TW, Everitt BJ. 2007. Forebrain connectivity of the prefrontal cortex in the marmoset monkey (Callithrix jacchus): an anterograde and retrograde tract-tracing study. J Comp Neurol [Internet] 502:86–112. Available from: http://www.ncbi.nlm.nih.gov/pubmed/17335041

Saleem KS, Kondo H, Price JL. 2008. Complementary circuits connecting the orbital and medial prefrontal networks with the temporal, insular, and opercular cortex in the macaque monkey. J Comp Neurol 506:659–693.

Seeley WW, Menon V, Schatzberg AF, Keller J, Glover GH, Kenna H, Reiss AL, Greicius MD. 2007. Dissociable intrinsic connectivity networks for salience processing and executive control. J Neurosci [Internet] 27:2349–2356. Available from: http://www.ncbi.nlm.nih.gov/pubmed/17329432

Sloniewski P, Usunoff KG, Pilgrim C. 1986. Diencephalic and mesencephalic afferents of the rat claustrum. Anat Embryol [Internet] 173:401–411. Available from: http://www.ncbi.nlm.nih.gov/entrez/query.fcgi?cmd=Retrieve&db=PubMed&dopt=Citation&list_uids=3963417

Smith JB, Alloway KD. 2014. Interhemispheric claustral circuits coordinate sensory and motor cortical areas that regulate exploratory behaviors. Front Syst Neurosci [Internet] 8. Available from: http://www.frontiersin.org/

Smith JB, Radhakrishnan H, Alloway KD. 2012. Rat claustrum coordinates but does not integrate somatosensory and motor cortical information. J Neurosci [Internet] 32:8583–8588. Available from: http://www.ncbi.nlm.nih.gov/pubmed/22723699

Smythies J, Edelstein L, Ramachandran V. 2012. Hypotheses relating to the function of the claustrum. Front Integr Neurosci [Internet] 6:53. Available from: http://www.ncbi.nlm.nih.gov/pubmed/22876222

Smythies J, Edelstein L, Ramachandran V. 2014. The Claustrum: Structural, Functional, and Clinical Neuroscience. San Diego, CA: Elsevier: Academic Press.

Squatrito S, Battaglini PP, Galletti C, Riva Sanseverino E. 1980. Projections from the visual cortex

to the contralateral claustrum of the cat revealed by an anterograde axonal transport method. Neurosci Lett 19:271–275.

Srinivasan R, Winter WR, Ding J, Nunez PL. 2007. EEG and MEG coherence: measures of functional connectivity at distinct spatial scales of neocortical dynamics. J Neurosci Methods [Internet] 166:41–52. Available from: http://www.ncbi.nlm.nih.gov/pubmed/17698205

Stam CJ. 2014. Modern network science of neurological disorders. Nat Rev Neurosci [Internet] 15:683–695. Available from: http://www.ncbi.nlm.nih.gov/pubmed/25186238

Torgerson CM, Van Horn JD. 2014. A case study in connectomics: the history, mapping, and connectivity of the claustrum. Front Neuroinform [Internet] 8:83. Available from: http://www.ncbi.nlm.nih.gov/pubmed/25426062

Ture U, Yasargil MG, Al-Mefty O, Yasargil DC. 2000. Arteries of the insula. J Neurosurg [Internet] 92:676–687. Available from: http://www.ncbi.nlm.nih.gov/pubmed/10761659

Vogt BA, Hof PR, Zilles K, Vogt LJ, Herold C, Palomero-Gallagher N. 2013. Cingulate area 32 homologies in mouse, rat, macaque and human: cytoarchitecture and receptor architecture. J Comp Neurol [Internet] 521:4189–4204. Available from: http://www.ncbi.nlm.nih.gov/pubmed/23840027

Watson GDR, Smith JB, Alloway KD. 2016. Interhemispheric connections between the infralimbic and entorhinal cortices: The endopiriform nucleus has limbic connections that parallel the sensory and motor connections of the claustrum. J Comp Neurol.

Wolf RC, Huber M, Depping MS, Thomann PA, Karner M, Lepping P, Freudenmann RW. 2013. Abnormal gray and white matter volume in delusional infestation. Prog Neuropsychopharmacol Biol Psychiatry [Internet] 46:19–24. Available from: http://www.ncbi.nlm.nih.gov/pubmed/23791615

Wu EL, Chen JH, Chiueh TD. 2010. Wideband MRI: theoretical analysis and its applications. Conf Proc IEEE Eng Med Biol Soc [Internet] 2010:5681–5684. Available from: http://www.ncbi.nlm.nih.gov/pubmed/21097317

Zhang XF, Li JC, Wen XD, Ren CG, Cai M, Chen CC. 2015. Susceptibility-Weighted Imaging of the Anatomic Variation of Thalamostriate Vein and Its Tributaries. PLoS One [Internet] 10:e0141513. Available from: http://www.ncbi.nlm.nih.gov/pubmed/26506095

Table and Figure Legends

Table 1: Case information and injection site targets for marmosets used in this study.

Figure 1: Top row: rostral, lateral, and schematic view of the marmoset claustrum reconstructed from Nissl stained coronal sections using the POSSUM software package (Majka et al., 2015). The thick blue line in each view shows the foreshortening of the rostral sections in the lateral view of the reconstruction, which is reflected in the heatmaps in later figures. The wireframe diagram in right-most panel shows the position of each section in the reconstructed view. The position of the section in the Nissl and myelin photos in the bottom row is indicated by the red line in each diagram. Bottom row: Nissl (left) and myelin (right) photos showing the claustrum (red dashed outline) in coronal section, and the adjacent putamen (Pu). Scale bars = 1mm.

Figure 2: Schematic diagram of injection sites. Illustration shows the medial wall of the anterior portion of the right cerebral hemisphere of an adult marmoset. Regional boundaries are as defined in the Paxinos et al. (2012) stereotaxic atlas. Abbreviations correspond to the case data shown in Table 1. Colored dots indicate the 2 dimensional position of the approximate center of each tracer injection, as reconstructed from histological sections.

Figure 3: Distribution of labelled cells in the ipsilateral claustrum and insular cortex following injection of cholera toxin B subunit conjugated to alexa 488 green fluorophore (CTB-alexa488) into area 32 of the left hemisphere in case CJ155. Cell body locations were plotted using an X-Y stage digitizer and the MD-Plot software package (see methods). Cells located outside the insula-claustrum region are not shown. The injection site and its position along the anterior-posterior axis are shown in the schematic diagram in the bottom center illustration. Red lines indicate the A-P level of each claustrum section (A-H), while the blue line indicates the level of the section containing the injection site. Every fourth section in the claustrum series is included in the figure, yielding an interslice interval of approximately 800 uM. The heat map in the lower right of the figure shows the relative density of labelled cells along the entire claustrum as reconstructed using the schematics shown in Figure 1. The normalized cell density is shown in the color-coded contour plot. Labelled cells were primarily located in two patches in the rostral and mid ventral claustrum. Numbers indicate approximate anterior-posterior stereotaxic coordinates based on the Paxinos et al. atlas (2012). OPAl- orbital periallocortex; OPro- orbital proisocortex; Gu- gustatory cortex; IPro- insular proisocortex; DI- disgranular insula; GI- granular insula.

Figure 4: Labelled cells in the claustrum and insula following a CTB-gold injection into area 32 of the right hemisphere of case CJ155. Figure conventions as in Figure 3.

Figure 5: Efferent projections to claustrum and insula following BDA injections into area 32 (Case CJ148-BDA). Terminal label density is not represented. A, B) Nissl-stained and dark field sections at the level of the BDA injection site. Cortical boundaries as identified by Nissl and myelin staining (not shown) are indicated by the arrowheads in A. C) Lateral schematic of the marmoset brain showing the A-P level of the injection site (blue line) and tissue sections in D-L (red lines). Numbers indicate approximate A-P stereotaxic level in Paxinos et al. (2012). D,G,J) Nissl stained tissue sections at the A-P levels indicated to the left. Red dashed boxes indicate the regions of high magnification shown in F,I, & L, and the black arrowheads indicate blood vessels used for section registration. The boundary of the claustrum is shown in blue in the photos in G and J. E,H,K) Bright field photos of BDA-reacted sections adjacent to the Nissl sections in D,G & J, showing the same blood vessels (arrowheads) and ROIs (red dashed boxes). Patches of terminal label are readily identified in E and H. F,I,L) High magnification bright field images showing axon terminals in OPro (F) and OPAl/claustrum (I). Negligible label is present in the agranular insula (L), though a few labelled terminals are evident in the claustrum.

Figure 6: Insula and claustrum label resulting from an injection of diamidino yellow (DY) into area 32V of the left hemisphere of case CJ148. Figure conventions as in Fig. 3. Scale bar = 1mm.

Figure 7: Insula and claustrum label resulting from an injection of DY into area 32V of the right hemisphere of case CJ132. Figure conventions as in Fig. 3. Scale bar = 1mm.

Figure 8: Differential thalamocortical projections to area 24b (A-E) and area 32V (F-J). Coronal sections through the most densely labelled regions of the thalamus from case CJ157-CTBg and case CJ148-DY. Thalamic area VA was most prominently labelled following injection into Area 24b, whereas injection into area 32V resulted in the vast majority of labelled cell bodies in the medio-dorsal nucleus of the thalamus (MD). Green dashed lines in the schematic drawing of the lateral view of the marmoset cortex at the bottom of the figure indicate the relative positions of the tissue sections shown in A-J above.

Figure 9: Distribution of labelled cell bodies in insula-claustrum region following CTB-g injection into area 24b/c of the right hemisphere in case CJ157. Pink lines in the lateral schematic

indicate the A-P positions of the tissue sections in A-G. Other figure conventions as in Fig. 3. Scale bar = 1mm.

Figure 10: Efferent projections to the insula-claustrum region resulting from injection of BDA into area 24d/23c (case CJ157-BDA). A) Darkfield photomicrograph of the approximate center of the injection site. B) Lateral schematic drawing showing the level of the tissue sections shown in D-L, relative to interaural zero (0). C) Brown shaded regions indicate terminal label fields identified by light microscopy. Terminal label density is not represented. The claustrum is shaded in blue. D,G,J) Nissl-stained sections showing the insula-claustrum regions and A-P coordinates of equivalent sections in the Paxinos et al. (2012) marmoset stereotaxic atlas. E,H,K) Bright field photomicrographs of BDA-reacted sections adjacent to those in D,G, & J. Red-dashed lines indicate the regions of higher magnification shown at left. F, I, L) High magnification bright field images showing axon terminal label in the disgranular and granular insula. Red arrow in L) indicates a retrogradely labelled cell body in the granular insula, reflecting partial retrograde transport of BDA from cortical targets. Scale bars = 1mm in left and center columns, 250 uM in right column.

Figure 11: "Shell neurons" in the ipsilateral extreme capsule following CTB-alexa488 injection into area 32. A) Dark field photomicrograph showing white matter tracts and cytoarchitectural boundaries of putamen, insula and claustrum. Dashed rectangle indicates region enlarged in panel B. Pink "X" characters indicate position of labelled neurons in panel B, relative to blood vessels (white arrowheads. B) Tiled confocal image of the marked region from panel A. The neurons in the lower left (small yellow arrows) are in the cytoarchitectonically defined claustrum, whereas the neuron in the upper center (pink arrows) are within the extreme capsule. Dashed rectangle indicates area of enlargement in panel C. C) Single confocal image slice from the series in panel B, showing a retrogradely labelled cell body in the external capsule (pink arrow), and a nearby blood vessel for reference (white arrowhead).

Animal ID	Sex	Age (y)	Body Weight (g)	Tracer
CJ133	M	2	320	DY
CJ148	M	3	430	DY
				BDA
CJ155	F	1.5	380	CTBa
				CTBg
CJ157	F	1.5	364	CTBg
				BDA

Hemisphere	Target	Transport (d)
Left	32v	6
Right	32v	10
Left	32	
Right	32	14
Left	32	
Left	24b/c	15
Right	24d/23a	

FIGURE 1

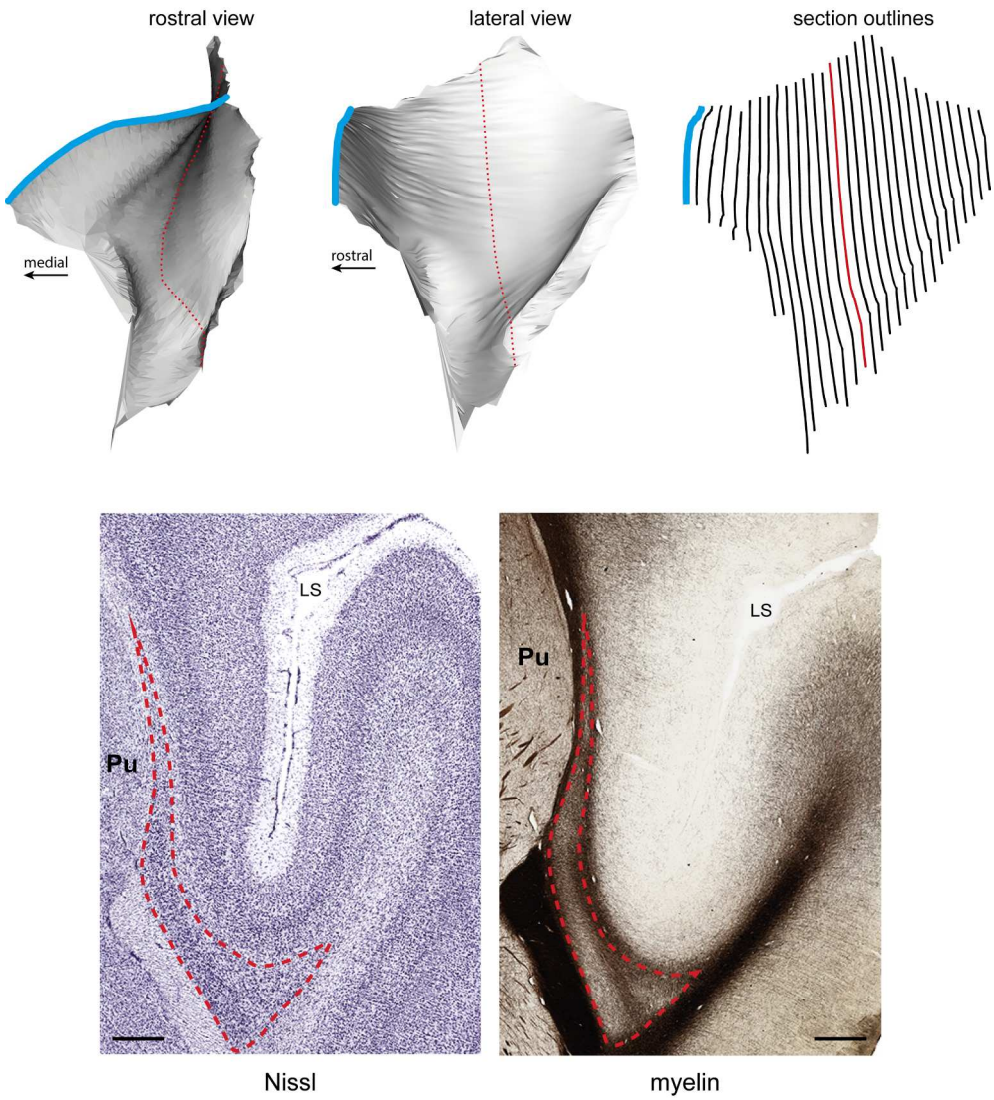

Figure 1: Top row: rostral, lateral, and schematic view of the marmoset claustrum reconstructed from Nissl stained coronal sections using the POSSUM software package (Majka et al., 2015). The thick blue line in each view shows the foreshortening of the rostral sections in the lateral view of the reconstruction, which is reflected in the heatmaps in later figures. The wireframe diagram in right-most panel shows the position of each section in the reconstructed view. The position of the section in the Nissl and myelin photos in the bottom row is indicated by the red line in each diagram. Bottom row: Nissl (left) and myelin (right) photos showing the claustrum (red dashed outline) in coronal section, and the adjacent putamen (Pu). Scale bars = 1mm.
199x242mm (300 x 300 DPI)

FIGURE 2

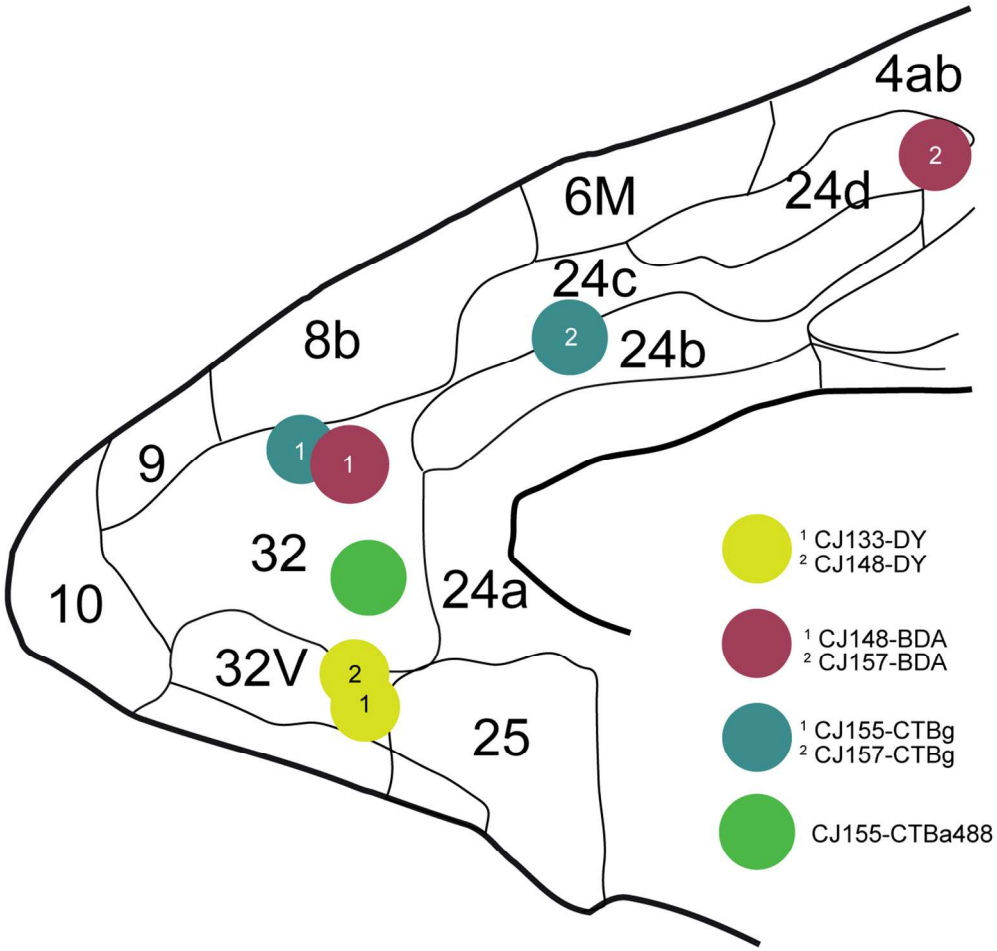

Figure 2: Schematic diagram of injection sites. Illustration shows the medial wall of the anterior portion of the right cerebral hemisphere of an adult marmoset. Regional boundaries are as defined in the Paxinos et al. (2012) stereotaxic atlas. Abbreviations correspond to the case data shown in Table 1. Colored dots indicate the 2 dimensional position of the approximate center of each tracer injection, as reconstructed from histological sections.
118x126mm (300 x 300 DPI)

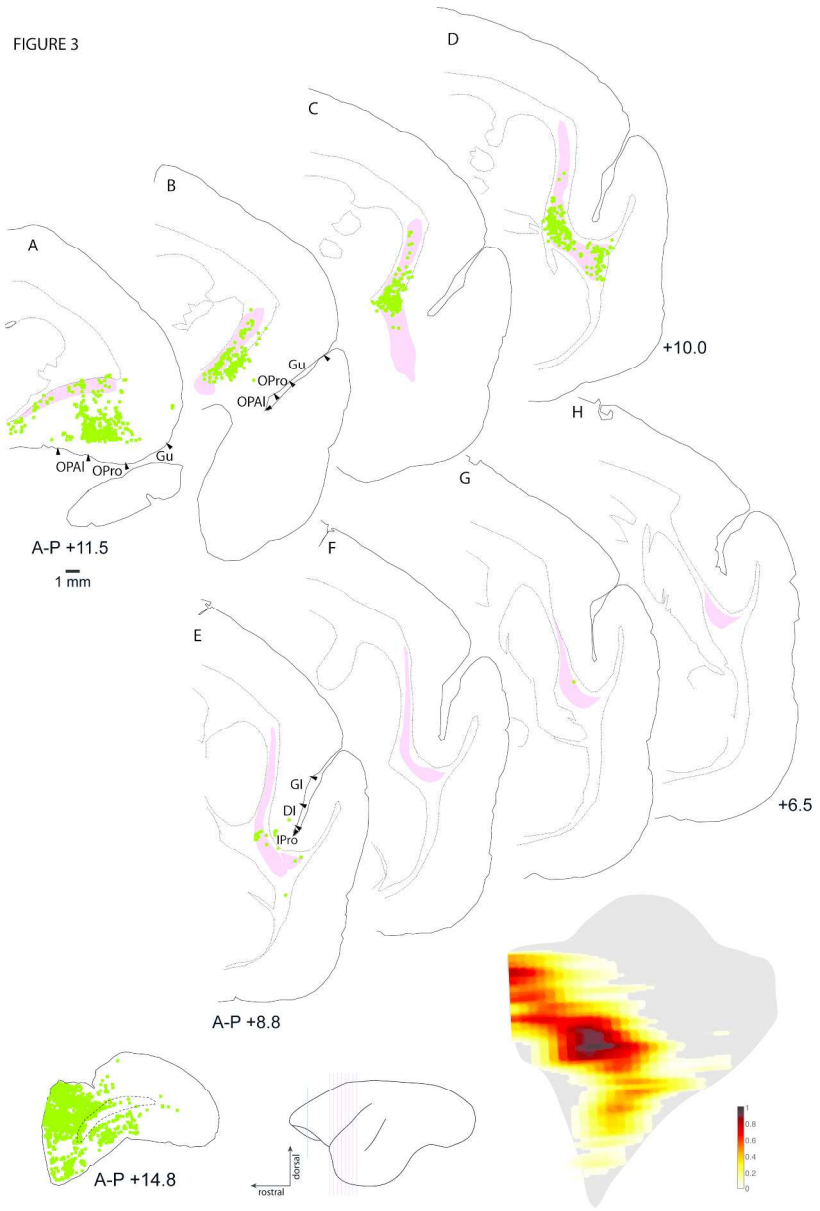

Figure 3: Distribution of labelled cells in the ipsilateral claustrum and insular cortex following injection of cholera toxin B subunit conjugated to alexa 488 green fluorophore (CTB-alexa488) into area 32 of the left hemisphere in case CJ155. Cell body locations were plotted using an X-Y stage digitizer and the MD-Plot software package (see methods). Cells located outside the insula-claustrum region are not shown. The injection site and its position along the anterior-posterior axis are shown in the schematic diagram in the bottom center illustration. Red lines indicate the A-P level of each claustrum section (A-H), while the blue line indicates the level of the section containing the injection site. Every fourth section in the claustrum series is included in the figure, yielding an interslice interval of approximately 800 uM. The heat map in the lower right of the figure shows the relative density of labelled cells along the entire claustrum as reconstructed using the schematics shown in Figure 1. The normalized cell density is shown in the color-coded contour plot. Labelled cells were primarily located in two patches in the rostral and mid ventral claustrum. Numbers indicate approximate anterior-posterior stereotaxic coordinates based on the Paxinos et al. atlas (2012). OPAl- orbital periallocortex; OPro- orbital proisocortex; Gu- gustatory cortex; IPro- insular

proisocortex; DI- disgranular insula; GI- granular insula.
194x290mm (300 x 300 DPI)

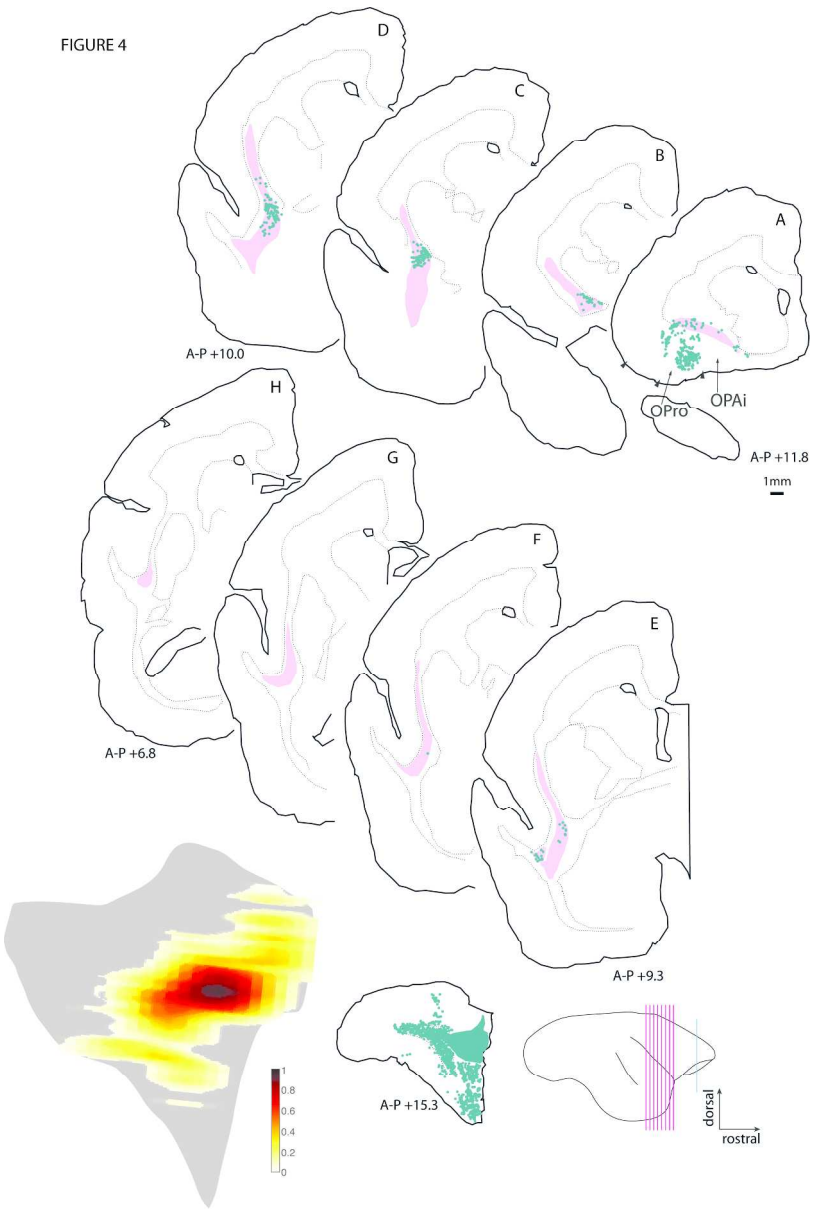

Figure 4: Labelled cells in the claustrum and insula following a CTB-gold injection into area 32 of the right hemisphere of case CJ155. Figure conventions as in Figure 3.
194x290mm (300 x 300 DPI)

FIGURE 5

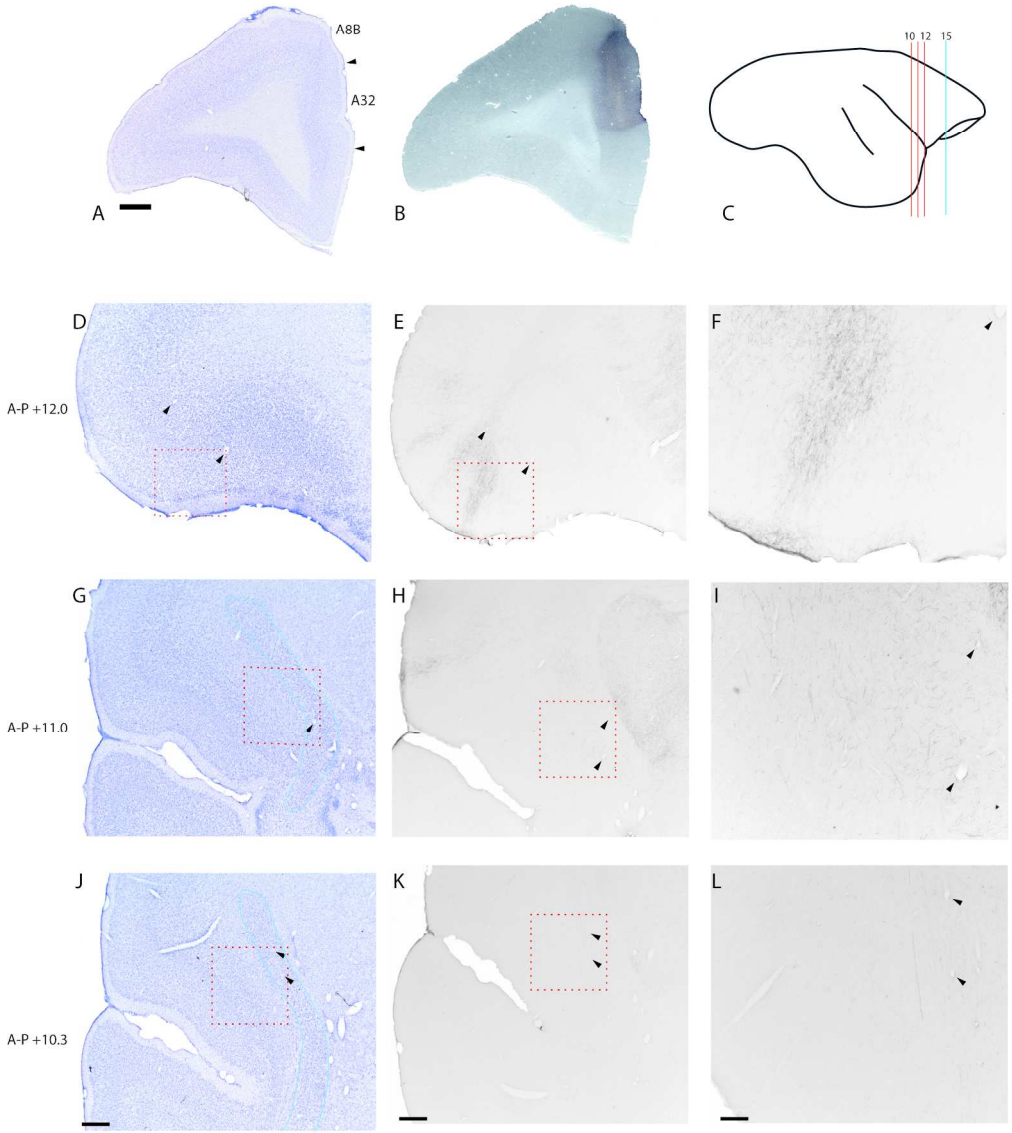

Figure 5: Efferent projections to claustrum and insula following BDA injections into area 32 (Case CJ148-BDA). Terminal label density is not represented. A, B) Nissl-stained and dark field sections at the level of the BDA injection site. Cortical boundaries as identified by Nissl and myelin staining (not shown) are indicated by the arrowheads in A. C) Lateral schematic of the marmoset brain showing the A-P level of the injection site (blue line) and tissue sections in D-L (red lines). Numbers indicate approximate A-P stereotaxic level in Paxinos et al. (2012). D,G,J) Nissl stained tissue sections at the A-P levels indicated to the left. Red dashed boxes indicate the regions of high magnification shown in F,I, & L, and the black arrowheads indicate blood vessels used for section registration. The boundary of the claustrum is shown in blue in the photos in G and J. E,H,K) Bright field photos of BDA-reacted sections adjacent to the Nissl sections in D,G & J, showing the same blood vessels (arrowheads) and ROIs (red dashed boxes). Patches of terminal label are readily identified in E and H. F,I,L) High magnification bright field images showing axon terminals in OPro (F) and OPAl/claustrum (I). Negligible label is present in the agranular insula (L), though a few labelled terminals are evident in the claustrum.

196x234mm (300 x 300 DPI)

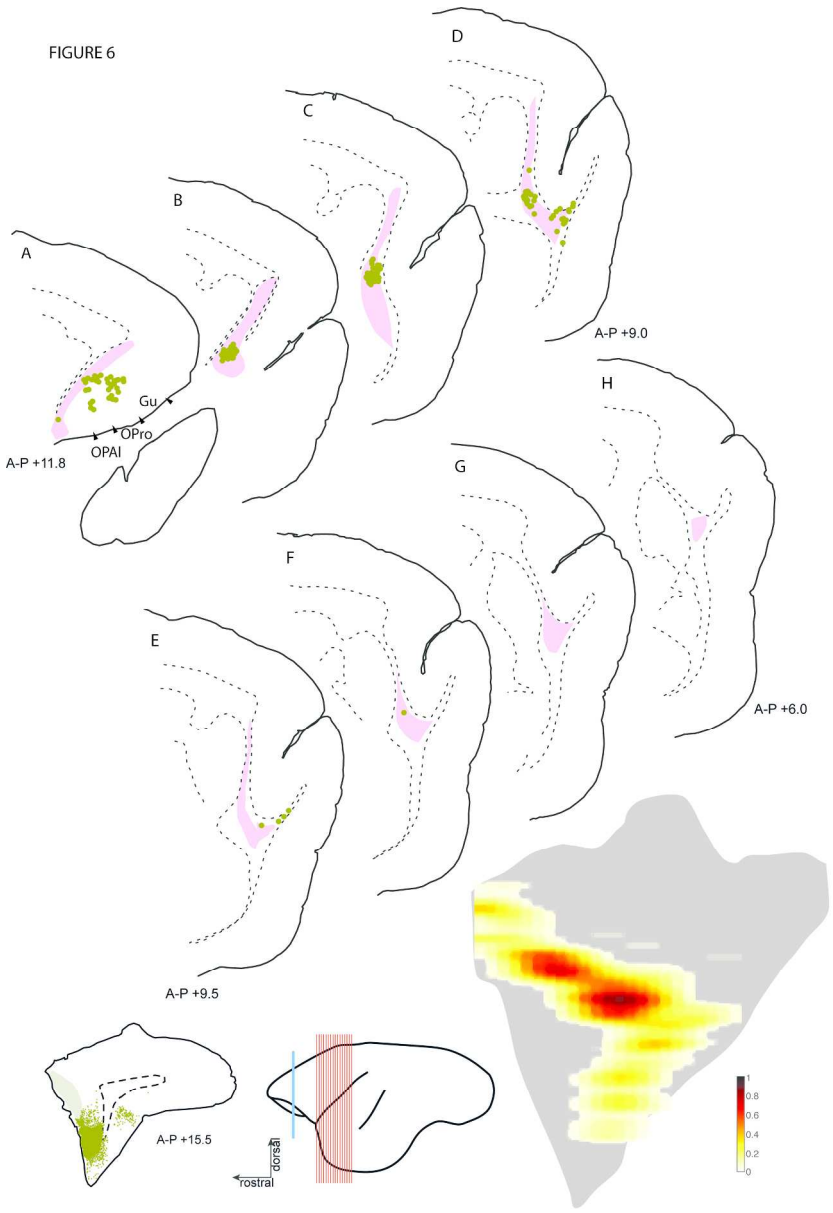

Figure 6: Insula and claustrum label resulting from an injection of diamidino yellow (DY) into area 32V of the left hemisphere of case CJ148. Figure conventions as in Fig. 3. Scale bar = 1mm.
199x288mm (300 x 300 DPI)

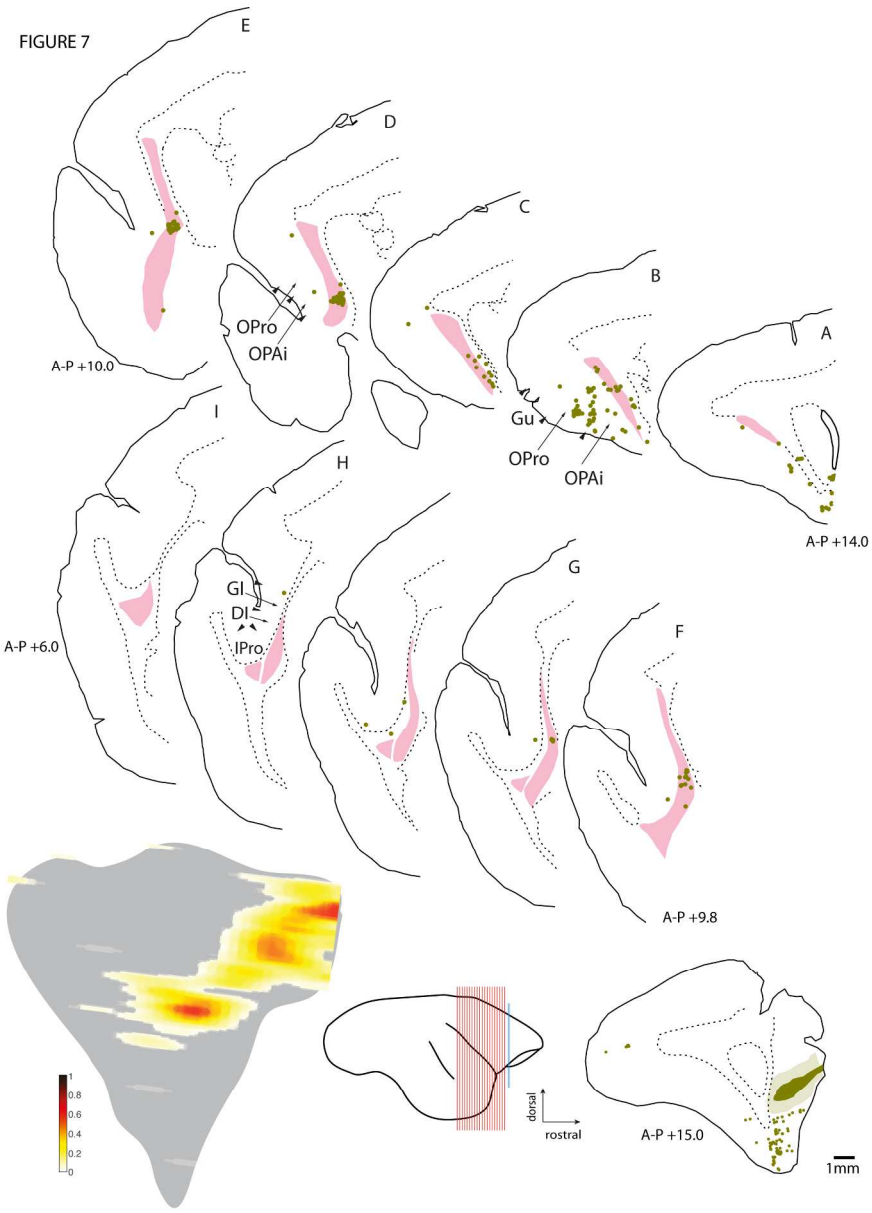

Figure 7: Insula and claustrum label resulting from an injection of DY into area 32V of the right hemisphere of case CJ132. Figure conventions as in Fig. 3. Scale bar = 1mm.
200x269mm (300 x 300 DPI)

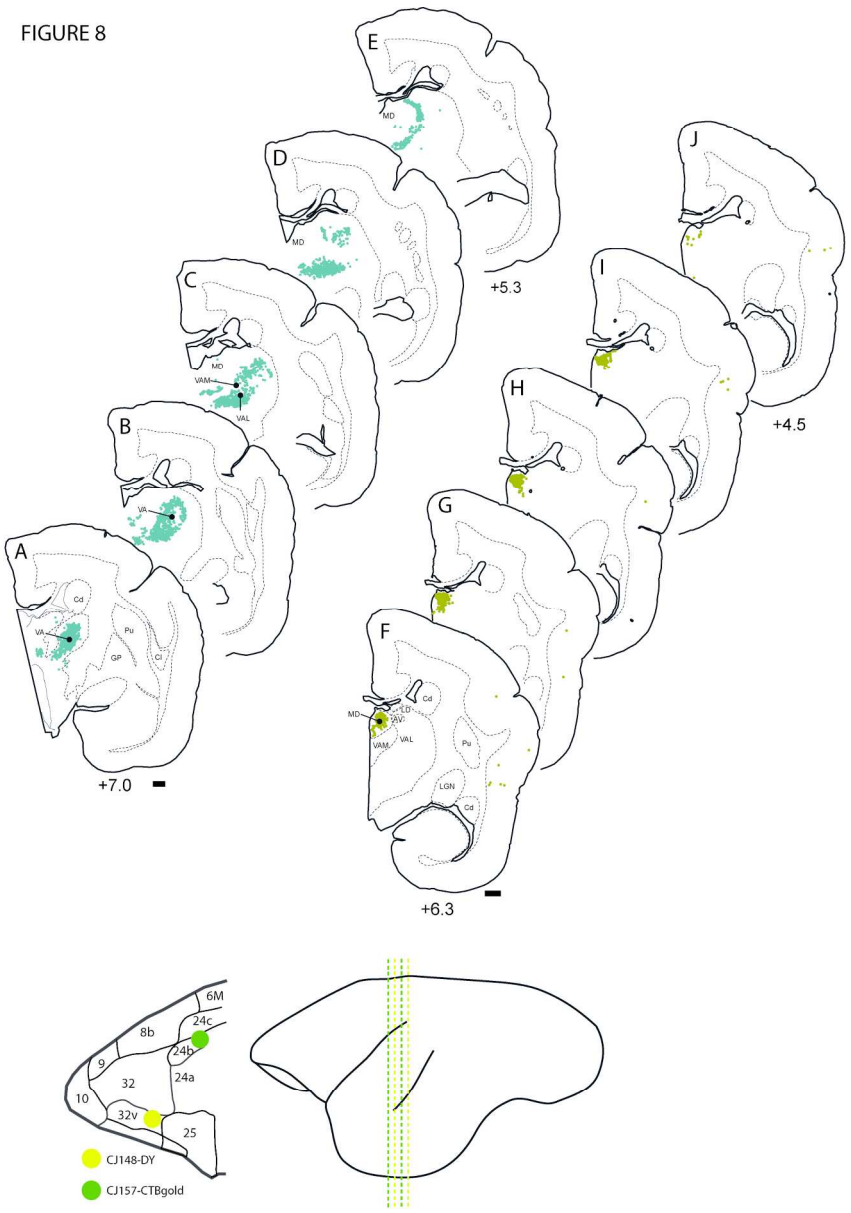

Figure 8: Differential thalamocortical projections to area 24b (A-E) and area 32V (F-J). Coronal sections through the most densely labelled regions of the thalamus from case CJ157-CTBg and case CJ148-DY. Thalamic area VA was most prominently labelled following injection into Area 24b, whereas injection into area 32V resulted in the vast majority of labelled cell bodies in the medio-dorsal nucleus of the thalamus (MD). Green dashed lines in the schematic drawing of the lateral view of the marmoset cortex at the bottom of the figure indicate the relative positions of the tissue sections shown in A-J above.
158x224mm (300 x 300 DPI)

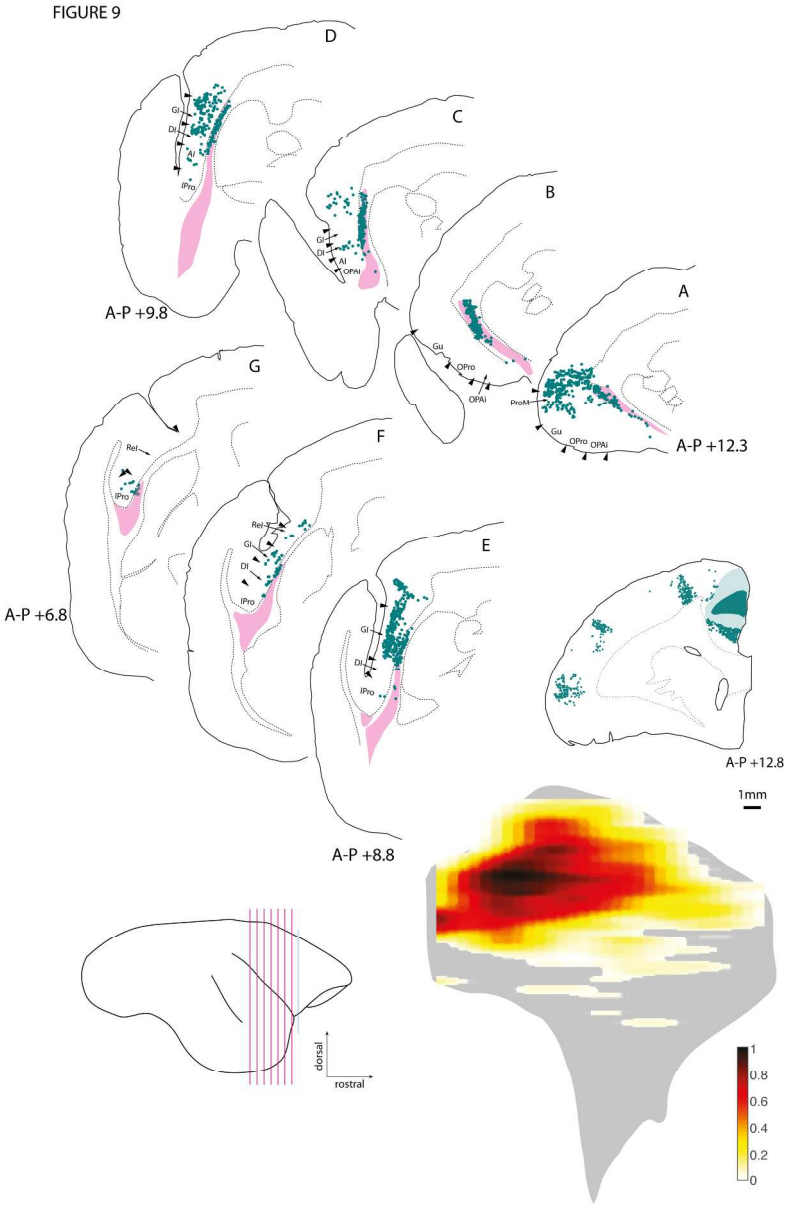

Figure 9: Distribution of labelled cell bodies in insula-claustrum region following CTB-g injection into area 24b/c of the right hemisphere in case CJ157. Pink lines in the lateral schematic indicate the A-P positions of the tissue sections in A-G. Other figure conventions as in Fig. 3. Scale bar = 1mm.
182x281mm (300 x 300 DPI)

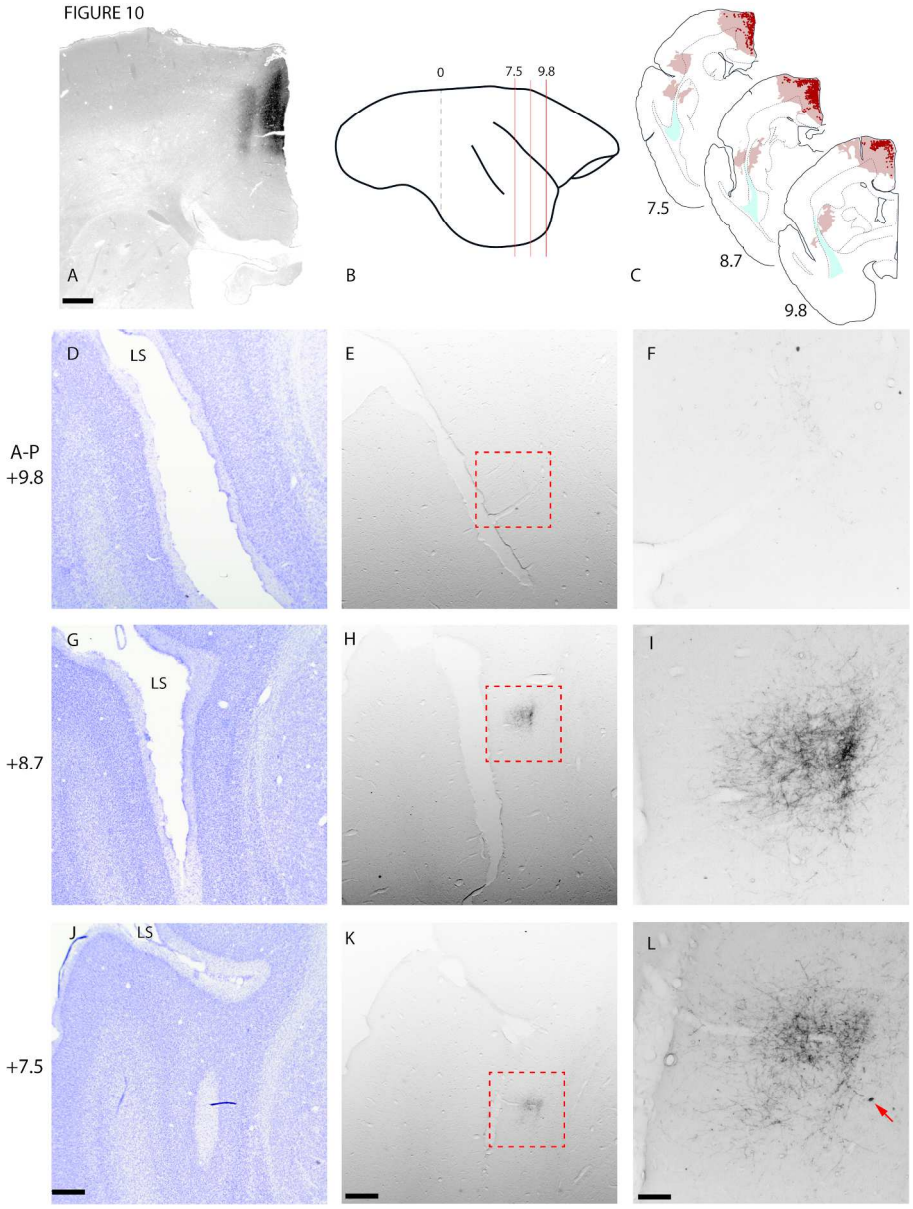

Figure 10: Efferent projections to the insula-claustrum region resulting from injection of BDA into area 24d/23c (case CJ157-BDA). A) Darkfield photomicrograph of the approximate center of the injection site. B) Lateral schematic drawing showing the level of the tissue sections shown in D-L, relative to interaural zero (0). C) Brown shaded regions indicate terminal label fields identified by light microscopy. Terminal label density is not represented. The claustrum is shaded in blue. D,G,J) Nissl-stained sections showing the insula-claustrum regions and A-P coordinates of equivalent sections in the Paxinos et al. (2012) marmoset stereotaxic atlas. E,H,K) Bright field photomicrographs of BDA-reacted sections adjacent to those in D,G, & J. Red-dashed lines indicate the regions of higher magnification shown at left.. F, I, L) High magnification bright field images showing axon terminal label in the disgranular and granular insula. Red arrow in L) indicates a retrogradely labelled cell body in the granular insula, reflecting partial retrograde transport of BDA from cortical targets. Scale bars = 1mm in left and center columns, 250 uM in right column.
203x270mm (300 x 300 DPI)

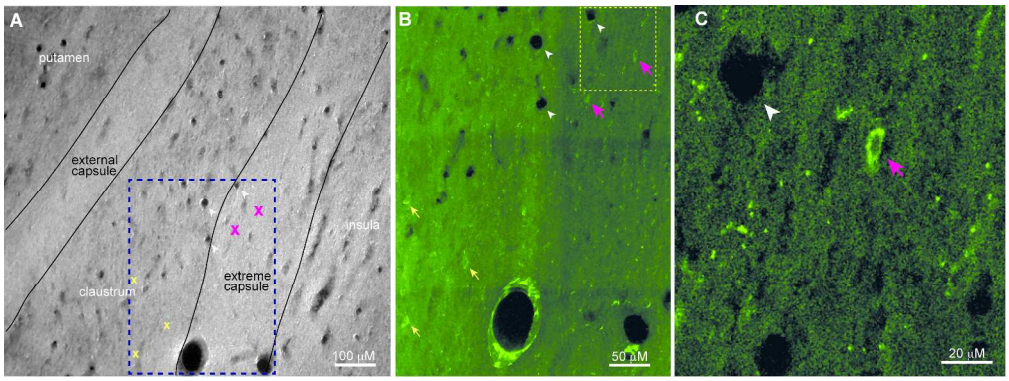

Figure 11: "Shell neurons" in the ipsilateral extreme capsule following CTB-alexa488 injection into area 32. A) Dark field photomicrograph showing white matter tracts and cytoarchitectural boundaries of putamen, insula and claustrum. Dashed rectangle indicates region enlarged in panel B. Pink "X" characters indicate position of labelled neurons in panel B, relative to blood vessels (white arrowheads. B) Tiled confocal image of the marked region from panel A. The neurons in the lower left (small yellow arrows) are in the cytoarchitectonically defined claustrum, whereas the neuron in the upper center (pink arrows) are within the extreme capsule. Dashed rectangle indicates area of enlargement in panel C. C) Single confocal image slice from the series in panel B, showing a retrogradely labelled cell body in the external capsule (pink arrow), and a nearby blood vessel for reference (white arrowhead).
334x124mm (300 x 300 DPI)

Graphical abstract:
Connections with the claustrum-insula region exhibit markedly different patterns between the medial prefrontal cortex and the anterior cingulate cortex of the marmoset following anterograde or retrograde tracer injections. Medial prefrontal connections are clustered in the medial and mid-ventral claustrum, with labelled neurons observed in the adjacent areas OPAl and Opro. In contrast, the anterior cingulate area 24b exhibits reciprocal connections with the dorsal and caudal regions of the claustrum, as well as the classical agranular, disgranular and granular insular areas.

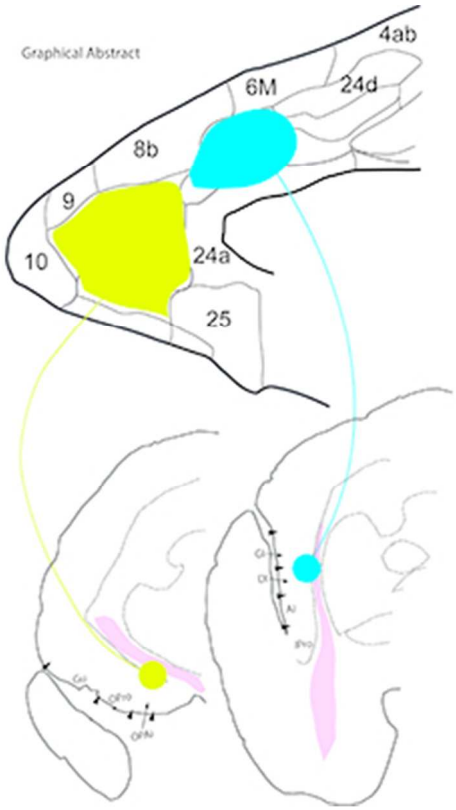

105x141mm (72 x 72 DPI)